# Unitary model for meson-nucleon scattering

T. Feuster[1,*] and U. Mosel[1,2]
[1]*Institut für Theoretische Physik, Universität Giessen, D-35392 Giessen, Germany*
[2]*Institute for Nuclear Theory, University of Washington, Box 351550, Seattle, Washington 98195*
(Received 29 August 1997)

We extract nucleon resonance parameters from an effective Lagrangian model employing the $K$-matrix approximation. To this end we analyze simultaneously all available data for reactions involving the final states $\pi N$, $\pi\pi N$, $\eta N$, and $K\Lambda$ in the energy range $m_N+m_\pi \leqslant \sqrt{s} \leqslant 1.9$ GeV. The background contributions are generated consistently from the relevant Feynman amplitudes, which significantly reduces the number of free parameters. The sensitivity of the parameters upon the $\pi N$–partial-wave analysis and the details of the Lagrangians and form factors used are discussed.
[S0556-2813(98)06306-7]

PACS number(s): 14.20.Gk, 11.80.Gw, 13.30.Eq, 13.75.Gx

## I. INTRODUCTION

A large number of models has been used in the past to obtain information about the excitation spectrum of the nucleon. The main problem faced is the multitude of open channels. A proper treatment of all of these channels requires both theoretical and numerical efforts. Furthermore, a large number of *a priori* unknown couplings is introduced. These can only be determined with some confidence if all available data are used. Ideally, all these data are decomposed into partial waves. Unfortunately, this has only been done so far for some reaction channels, namely, $\pi N \to \pi N$, $\pi N \to \pi\pi N$, and $\gamma N \to \pi N$. For the other possible channels there are only total and differential cross section and polarization data available.

A large group of models uses only hadronic data to extract resonance parameters [1–4] since meson photoproduction only allows for the determination of the product of the hadronic and electromagnetic couplings [5]. All these models employ interaction potentials constructed to fulfill unitarity and analyticity. The main difference between these models is the treatment of the reaction channels. In [4] all inelastic channels are summed up in a ''generic'' $\pi\Delta$ channel, whereas in [3] both $\pi N \to \pi N$ and $\pi N \to \pi\pi N$ data are fitted. In other studies [6,7] the $\pi N \to \eta N$ data are also used and the $\pi\pi N$ decays of the resonances are included by means of an effective $\zeta$ meson. It is clear that higher-lying resonances might also have other decay channels like $K\Lambda$ and $K\Sigma$ [8]. The corresponding couplings have so far not been extracted from a multichannel calculation.

The $S_{11}(1535)$ resonance has long been of special interest because of its large $\eta N$ branching ratio. This value of about 50% is not well understood in models of the nucleon and resonances [9–11].[1] Recently, a description of the $S_{11}(1535)$ as a quasibound $K\Sigma$ state has been put forward [12]. An accurate extraction of the $S_{11}(1535)$ parameters would therefore constrain models of the structure of the nucleon. Unfortunately, the values for the mass and decay widths ($m_R$ = 1.526–1.553 GeV, $\Gamma_\pi$=20–84 MeV, $\Gamma_\eta$=54–91 MeV) found in different works vary strongly. As we will see, this is mainly due to the poor $\pi N \to \eta N$ data.

To improve this situation, information from photoproduction experiments might be used. As a result of the rescattering, these data cannot be analyzed independently, but a combined model for the hadronic and electromagnetic channels is needed. First attempts have been made in the $\Delta$ region of pion photoproduction [13,14]. There unitarity was guaranteed by using the $K$-matrix approximation. For higher energies mainly effective Lagrangian models [5,15] have been used to extract information on the hadronic and electromagnetic couplings. While these models have been rather successful, no attempt has been made so far to describe the hadronic final state interaction for all possible channels using *the same Lagrangians* as for the photoproduction reactions.

As a first step in this direction we have developed a model for both meson-nucleon and photon-nucleon reactions, starting from effective Lagrangians which is unitary and includes a large number of reaction channels. In this paper we present the results for the resonance masses and widths as extracted from fits to the available hadronic data. By using a speed plot technique described by Höhler [16] we estimate the poles and residues of the resonances. In doing so we bypass a direct calculation of the $T$ matrix in the complex energy plane, since the technical effort needed for an analytic continuation of all Feyman amplitudes is beyond the scope of this paper. Since our main interest is the determination of the hadronic couplings of the known resonances, we furthermore do not search for additional states as was done, e.g., by Manley and Saleski [3].

This paper is organized as follows: First the reactions included and the available data are listed. Then we give an overview of the model used. This overview consists of a short discussion of the $K$-matrix approximation and the Lagrangians. We show the results of our fits in comparison to the experimental data and compare the extracted values of the masses and partial widths to other works.

*Electronic address: Thomas.Feuster@theo.physik.uni-giessen.de

[1]Capstick and Roberts [9] are able to reproduce the $\pi N$ and $\eta N$ branching ratios but overestimate the partial decay widths by more than 50%. Glozman and Riska [10] explain the $\eta N$ branching ratio of the $S_{11}(1535)$ by the flavor-spin symmetry of the quark wave functions, whereas Bijker *et al.* [11] suggest that the large $\eta N$ width of the $S_{11}(1535)$ ''is not due to a conventional $q^3$ state.''

 

## II. REACTION CHANNELS AND DATABASE

The reaction channels in the energy range up to $\sqrt{s} = 1.9$ GeV, to which we restrict ourselves in this paper, are $\pi N \to \pi N$, $\pi N \to \pi\pi N$, $\pi N \to \eta N$, $\pi N \to K\Lambda$, and $\pi N \to K\Sigma$. In order to keep our model as simple as possible, yet at the same time use a maximum amount of information, we adopt the following strategy.

(i) $\pi N \to \pi N$: Two widely used partial wave analyses (PWA) are available for this reaction. One is the older analysis by Höhler *et al.* [2]; the other is the latest version from the VPI group (SM95 [4]). Recently (cited in [6]), Höhler (KA84 [2]) has suggested to use the solution SM95 in the $S_{11}$ channel below the $\eta N$ threshold in order to account for new experimental data. We will present fits using both the KA84 and the SM95 PWA. This allows us to check the dependence of the parameters on the analysis used. Unfortunately, no error bars have been given for the solution KA84. Since knowledge of the uncertainties is essential for all fitting procedures, errors have to be assigned to these data by hand. This assignment involves a certain arbitrariness. For example, Batinić *et al.* have chosen an error that grows linearly with energy from some minimal value [6]. In the present work we use a different prescription:

$$\Delta T_\alpha(W_i) \equiv \max(0.03 T_\alpha(W_i), 0.015), \tag{1}$$

so that each data point $i$ at an energy $W_i$ in a partial wave $T_\alpha$ carries an error of at minimum 3%. The main assumption behind this choice is that the errors are of the order of those of the SM95 data. Only then is a comparison of the resulting $\chi^2$ values meaningful. A change in the exact numbers in Eq. (1) does not have a sizable influence on the final parameters; it merely sets the scale for the $\chi^2$ values of the fits.

(ii) $\pi N \to \pi\pi N$: Manley and Saleski [3] performed a decomposition of the available data with respect to various intermediate states like $\pi\Delta$, $\pi P_{11}(1440)$, and $\rho N$. In order to keep the model as simple as possible we do not treat all these states explicitly, but follow a more phenomenological approach [6,7]: the $\pi\pi N$ decay is parametrized by the coupling to a scalar, isovector $\zeta$ meson with mass $m_\zeta = 2m_\pi$. We have chosen isovector instead of isoscalar (as in [7]), to also allow for the decays of $I = \frac{3}{2}$ resonances into $\pi\pi N$. To determine the couplings from the results of Manley and Saleski we use their total $\pi N \to \pi\pi N$ cross sections for the different partial waves.

(iii) $\pi^- p \to \eta n$: Measurements of the total and differential cross sections have been performed by several groups over a wide energy range. Unfortunately, some of these measurements do not agree very well with the others. Batinić *et al.* [6] have proposed a scheme to incorporate these discrepancies by enlarging the error for some of the data points. This scheme has also been used here. As will be seen, the large uncertainties in the data for this channel do not allow for a reliable determination of the $S_{11}(1535)$ parameters and the $\eta N$-scattering length.

(iv) $\pi^- p \to K^0\Lambda, K\Sigma$: These channels are of minor importance. Only the $K\Lambda$ gives a significant contribution to the inelastic cross section around 1.7 GeV. Therefore, we only include this reaction in our work. The observables used are the total and differential cross sections and $\Lambda$ polarizations. Because of the large errors, the latter play only a minor role and are included for completeness only. A detailed description of all channels containing strange particles in the final state is not possible, since there is a coupling to the hyperon spectrum through $u$-channel contributions in this case. A determination of the parameters of hyperon resonances is clearly beyond the scope of this work because it would require the inclusion of further reactions like $KN \to KN$.

We also neglect channels that lead to final states containing more than two pions (e.g., $\pi N \to \omega N \to \pi\pi\pi N$). In their analysis Manley and Saleski found missing inelasticity only for some resonances. To account for this, they introduced effective $\omega N$ and $\rho\Delta$ channels that lead to three-pion final states. Therefore, the partial widths extracted there can only be viewed as upper bounds for these additional decay channels. In our case only the $P_{13}(1720)$ is affected by this. As will be discussed in Secs. V B and VI B, we do not treat these additional channels explicitly, but fit the parameters of this resonance without the $\pi\pi N$ data.

## III. *K*-MATRIX APPROXIMATION

To solve the coupled Bethe-Salpeter equations encountered in meson-nucleon scattering a number of models has been proposed. For completeness we give a short summary of the most important ones. For a more detailed discussion the reader is referred to the literature.

(1) In the widely used ansatz of Cutkosky *et al.* (the so-called Carnegie-Mellon Berkeley or CMB ansatz, also used by Batinić *et al.*) [1,6] the $T$ matrix in a given channel is assumed to be a sum over the contributions from a number of intermediate particles. The coupling $f(s)$ of the asymptotic states to these particles determines the imaginary part of the phase factor $\Phi(s)$:

$$T_{ab} = \sum_{i,j}^{N} f_a(s)\sqrt{\rho_a}\gamma_{ai} G_{ij}(s)\gamma_{jb}\sqrt{\rho_b} f_b(s),$$

$$\mathrm{Im}\ \Phi_a(s) = [f_a(s)]^2 \rho_a, \tag{2}$$

with $\rho_a = q_a/\sqrt{s}$. The real part of $\Phi_a(s)$ is then calculated from a dispersion relation, thus ensuring analyticity. With this phase factor the self-energy $\Sigma(s)$ and the dressed propagator $G(s)$ are taken to be

$$\Sigma_{kl}(s) = \sum_a \gamma_{ka}\Phi_a(s)\gamma_{al},$$

$$G_{ij}(s) = G^0_{ij}(s) + \sum_{k,l}^{N} G^0_{ik}(s)\Sigma_{kl}(s)G_{lj}(s). \tag{3}$$

$\gamma_{ab}$ denote the free coupling parameters that are fitted to the data. Besides the known resonance contributions to $T_{ab}$ the background is included via additional terms with poles below the $\pi N$ threshold. The number of background parameters is therefore proportional to the number of orthogonal channels included in the calculation.

One advantage of this formalism is that it is easy to determine the complex poles of the $T$ matrix since the potential is separable and depends only on $s$. As inelastic channels $\eta N$, $\rho N$, $\pi\Delta$, $\pi P_{11}(1440)$, $\epsilon N$, $\omega N$, and $\rho\Delta$ have been

taken into account. Furthermore, information on the $\eta N$ threshold production amplitude was used in the fits.

(2) Manley and Saleski [3] start from an $S$ matrix which is written as a product of background and resonant terms:

$$S = S_R^T S_B S_R,$$

$$S_B = \frac{1+iK_B}{1-iK_B}, \quad S_R = \prod_k^N S_k^{1/2}. \tag{4}$$

$S_k^{1/2}$ stands for the contribution of the $k$th resonance and is related to the $T$ matrix by

$$S_k^{1/2} = 1 + [i - x_k + (1+x_k^2)^{1/2}]T_k, \quad S_k = 1 + 2iT_k, \tag{5}$$

which in turn is assumed to have a Breit-Wigner form. The $n$-channel background $K_B$ is parametrized in terms of $n$ independent linear functions of $\sqrt{s}$. The inelastic channels included are the same as in the model of Cutkosky *et al.*

(3) The $K$-matrix approximation amounts to setting $K = V$ instead of the full Bethe-Salpeter equation [7,17]

$$K = V + V\ \mathrm{Re}(G_{\mathrm{BS}})K,$$

$$T = K - iK\ \mathrm{Im}(G_{\mathrm{BS}})T. \tag{6}$$

This corresponds to a special choice for the Bethe-Salpeter propagator $G_{\mathrm{BS}}$ ($k_N$ and $k_m$ are the nucleon and meson four-momentum, respectively),

$$G_{\mathrm{BS}} = -2i(2\pi)^2 m_N \delta(k_N^2 - m_N^2)\,\delta(k_m^2 - m_m^2) \times \theta(k_N^0)\,\theta(k_m^0)(\not{k}_N + m_N) \tag{7}$$

and leads to a rather simple equation for $T$:

$$T = \frac{V}{1-iV}. \tag{8}$$

Besides Hermiticity no further constraints on the potential $V$ are needed. This simple form makes the $K$-matrix approximation most suitable for numerical computation.

As stated in the Introduction, we want to construct the interaction potential $V$ starting from effective Lagrangians that describe the couplings between all involved particles. The main advantage of this ansatz is that the background contributions are calculated from the same Feynman diagrams as the resonant amplitudes. This reduces the number of parameters drastically, since it is now only proportional to the number of diagrams contributing to the background. It is also straightforward to incorporate various aspects like chiral symmetry by choosing the proper $\pi N$ Lagrangian.

The main drawback of this approach is that the special choice for $G_{\mathrm{BS}}$ used in Eq. (8) violates analyticity. Because of the complicated functional form of $V$ in the effective Lagrangian ansatz, it is not an easy task to restore analyticity by the use of dispersion relation integrals (as is done in the CMB ansatz). Since this paper is meant to serve as a basis for further investigations using effective Lagrangians, we do not attempt to go beyond the $K$-matrix approximation here.

In order to test the $K$-matrix approximation Pierce and Jennings [17] fitted the $\pi N$-phase shifts also using other intermediate propagators. They found no significant differences in the extracted parameters. It thus seems that all the physically relevant contributions are already contained in Eq. (8).

## IV. DESCRIPTION OF THE MODEL

In an effective Lagrangian model the potential $V$ is specified in terms of couplings between different particles. In our case these are the nucleon, the $\Lambda$, nucleon resonances, and mesons. We take into account $s$-, $u$-, and $t$-channel contributions[2] which can be represented by the usual Feynman diagrams. Only in the case of $K\Lambda$ do we disregard the $u$-channel contributions since these would involve hyperon resonances which we do not include. As mentioned above, in this framework the background consists of all diagrams that do not involve nucleon resonances. This limits the number of free parameters considerably and puts additional constraints on the resonance parameters, since the background contributions to the individual partial waves are no longer independent of each other.

In this work we limit ourselves to partial waves with spin $\frac{1}{2}$ and $\frac{3}{2}$. We include all corresponding nucleon resonances, except for the $P_{31}(1750)$ which only has a one-star status [8]. For the resonances with spin $\frac{1}{2}$ and $\frac{3}{2}$ the Lagrangians can be given in an unambiguous way [18,19], even though we already have to include additional parameters to describe the off-shell couplings of spin-$\frac{3}{2}$ resonances. Because we cannot account for contributions of higher partial waves to total and differential cross sections, we are limited to an energy range $\sqrt{s} \leqslant 1.9$ GeV. This value was chosen to allow for a fit of each resonance contribution below and above the resonance positions. Fortunately, the resonances omitted here [$D_{15}(1675)$ and $F_{15}(1680)$] are known to have only a small branching ratio into the $\eta N$ and $K\Lambda$ channels [6,20], so that they do not have a strong influence on the fits to the $\pi^- p \to \eta n$ and $\pi^- p \to K^0\Lambda$ data.

### A. Background contributions

It is well known [21] that the $\pi N$-scattering length can be calculated in the linear $\sigma$ model [22]. There, chiral symmetry is guaranteed through inclusion of the scalar, isoscalar $\sigma$ meson. The couplings of $\pi$ and $\sigma$ to the nucleon are fixed and depend only on the nucleon mass and the pion decay constant. In this work we use the nonlinear $\sigma$ model for guidance in constructing the coupling terms for two reasons: (i) the $\sigma$ meson is not observed in nature, and (ii) in the linear model additional terms are needed to fulfill the low-energy theorems of pion photoproduction [5,7] because it has pseudoscalar (PS) instead of pseudovector (PV) $\pi N$ coupling. In the nonlinear $\sigma$ model the coupling of the nucleons

[2] In principle, there is the problem of ''double counting'' if one includes all resonances in the $s$-channel along with all $t$-channel diagrams. The assumption is that the relatively small number of contributions taken into account in the $t$ channel minimizes double counting. The validity of this assumption can only be investigated in a quantitative way once dispersion relations are considered. This has to be examined in further investigations.

TABLE I. Masses and widths of the mesons included. $\pi$, $\zeta$, $\eta$, and $K$ are the asymptotic states. Data as given by the Particle Data Group [8].

| | $M$ [GeV] | $S$ | $I$ | $P$ | $\Gamma_{\text{tot}}$ [MeV] | $\Gamma_{\pi\pi}$ [%] | $\Gamma_{\pi\eta}$ [%] | $\Gamma_{\pi k}$ [%] | $\Gamma_{\pi\gamma}$ [%] | $\Gamma_{\eta\gamma}$ [%] | $\Gamma_{k\gamma}$ [%] | $\Gamma_{\gamma\gamma}$ [%] |
|---|---|---|---|---|---|---|---|---|---|---|---|---|
| $\pi$ | 0.139 | 1 | 1 | – | 7.85 [a] | 0 | 0 | 0 | 0 | 0 | 0 | 99 |
| $\zeta$ [c] | 0.278 | 1 | 1 | + | – | – | – | – | – | – | – | – |
| $\eta$ | 0.548 | 0 | 0 | – | 1.2 [b] | 0 | 0 | 0 | 0 | 0 | 0 | 39 |
| $K$ [c] | 0.498 | 0 | $\frac{1}{2}$ | – | – | – | – | – | – | – | – | – |
| $\rho$ | 0.769 | 1 | 1 | – | 0.151 | 100 | 0 | 0 | 0.05 | 0.04 | 0 | 0 |
| $a_0$ | 0.983 | 0 | 1 | + | 0.200 | 0 | 100 | 0 | 0 | 0 | 0 | 0 |
| $K^*$ | 0.892 | 1 | $\frac{1}{2}$ | – | 0.050 | 0 | 0 | 100 | 0 | 0 | 0.1 | 0 |

[a] $\pi^0$ width in eV.
[b] Width in keV.
[c] No decays were taken into account.

and the pseudoscalar mesons to the vector mesons can then be obtained by introducing the latter as massive gauge particles [23]. In addition to the vector coupling we also include the $\rho NN$ tensor coupling. As in other effective Lagrangian approaches this mimics the breaking of chiral symmetry [5]. Besides these couplings we also have the contributions from other scalar ($a_0$) and vector ($K^*$) mesons so that the total Lagrangian for the nonresonant contributions is (suppressing isospin factors here and in the following)

$$\begin{aligned}\mathcal{L}_{\text{NR}} = & -\frac{g_{\varphi NN}}{2m_N}\bar{N}\gamma_5\gamma_\mu(\partial^\mu\varphi)N - g_{sNN}s(\bar{N}N) - g_{s\varphi\varphi}s(\varphi^*\varphi) \\ & - g_{vNN}\bar{N}\left(\gamma_\mu v^\mu - \kappa_v\frac{\sigma_{\mu\nu}}{4m_N}v^{\mu\nu}\right)N \\ & - g_{v\varphi\varphi}[\varphi\times(\partial_\mu\varphi)]v^\mu. \end{aligned} \tag{9}$$

Here $\varphi$ denotes the asymptotic mesons $\pi$, $\eta$, and $K$. A coupling of the nucleon to the $\zeta$ meson is not taken into account. $s$ and $v$ are the intermediate scalar and vector mesons ($a_0$, $\rho$, and $K^*$) and $v^{\mu\nu}=\partial^\nu v^\mu - \partial^\mu v^\nu$ is the field tensor of the vector mesons; $N$ is either a nucleon or a $\Lambda$ spinor. For the $I=1$ mesons ($\pi$, $\zeta$, and $\rho$) $\varphi$ and $v^\mu$ need to be replaced by $\boldsymbol{\tau}\cdot\boldsymbol{\varphi}$ and $\boldsymbol{\tau}\cdot\boldsymbol{v}^\mu$ in the $\varphi,vNN$ couplings and by $\boldsymbol{\varphi}$ and $\boldsymbol{v}^\mu$ otherwise. As we will see later on, the influence of $a_0$ is small, whereas $K^*$ gives the dominant contribution to $\pi^- p \to K^0\Lambda$ at higher energies. The parameters used for the mesons are taken from [8] and listed in Table I.

### B. Resonance couplings

For the coupling of spin-$\frac{1}{2}$ resonances to the mesons we again have the choice between PS and PV coupling. In principle one could start with a linear combination of both and fit the ratio PS/PV to the data. To keep the number of parameters small, we choose PS coupling for all negative parity resonances and PV for positive parity. For the negative parity case this is done in accordance with the calculation of Deutsch-Sauermann *et al.* [7]. For positive parity states we choose, as for the nucleon, PV rather than PS, thus circumventing the need for additional scalar mesons to reproduce the scattering lengths.

For the $S_{11}$ and $S_{31}$ resonances we therefore have

$$\mathcal{L}^{\text{PS}}_{\varphi NR_{1/2}} = -g_{\varphi NR}\bar{R}\Gamma\varphi N + \text{H.c.}, \tag{10}$$

and in the case of $P_{11}$ and $P_{31}$ the couplings are given by

$$\mathcal{L}^{\text{PV}}_{\varphi NR_{1/2}} = -\frac{g_{\varphi NR}}{m_R \pm m_N}\bar{R}\Gamma_\mu(\partial^\mu\varphi)N + \text{H.c.}, \tag{11}$$

with the upper sign for positive parity. The vertex operators $\Gamma$ and $\Gamma_\mu$ depend on the parity of the particles involved. For a meson with negative intrinsic parity coupled to two baryons with positive parity (e.g., $\pi NN$) they are given by $\Gamma = i\gamma_5$ and $\Gamma_\mu = \gamma_5\gamma_\mu$. Otherwise [e.g., for $\pi NS_{11}(1535)$] we have $\Gamma = 1$ and $\Gamma_\mu = i\gamma_\mu$.

For the spin-$\frac{3}{2}$ resonances the following coupling is used:

$$\mathcal{L}_{\varphi NR_{3/2}} = \frac{g_{\varphi NR}}{m_\pi}\bar{R}^\alpha\Theta_{\alpha\mu}(z_\varphi)\Gamma(\partial^\mu\varphi)N + \text{H.c.},$$

$$\Theta_{\alpha\mu}(z) = g_{\alpha\mu} - \frac{1}{2}(1+2z)\gamma_\alpha\gamma_\mu, \tag{12}$$

again with a vertex operator $\Gamma$, which is 1 or $\gamma_5$, depending on the parity of the involved particles.

The operator $\Theta_{\alpha\mu}(z)$ allows us to vary the off-shell admixture of spin-$\frac{1}{2}$ fields. Some attempts have been made to fix the parameters $z$ by examining the Rarita-Schwinger equations and the transformation properties of the interaction Lagrangians [24,18]. Unfortunately, the measured pion-photoproduction data and $\Delta N\gamma$-transition strength cannot be explained using these results [13]. Therefore, we follow Benmerrouche *et al.* [5] and others who treat the $z$'s as free parameters and determine them by fitting the data. For a detailed discussion of the coupling of spin-$\frac{3}{2}$ particles and the problems encountered there see [19].

For the isovector mesons $\pi$ and $\zeta$, the field $\varphi$ in Eqs. (10)–(12) needs to be replaced by $\boldsymbol{\tau}\cdot\boldsymbol{\varphi}$ for $I=\frac{1}{2}$ resonances and by $\boldsymbol{T}\cdot\boldsymbol{\varphi}$ otherwise.

### C. Form factors

In order to reproduce the experimental data form factors have to be introduced. They are meant to model the deviations from the pointlike couplings (9)–(12) due to the quark

structure of nucleons and resonances. Because it is not clear *a priori* which form these additional factors should have, they introduce a source of systematical error in all models. As we have already shown for the case of pion photoproduction [15], the parameters extracted can depend strongly on the functional form used for the form factors. To investigate this dependence we use three different form factors in our fits:

$$F_p(q^2)=\frac{\Lambda^4}{\Lambda^4+(q^2-m^2)^2},$$

$$F_e(q^2)=\exp\left(-\frac{(q^2-m^2)^2}{\Lambda^4}\right),$$

$$F_t(q^2)=\frac{\Lambda^4+(q_t^2-m^2/2)^2}{\Lambda^4+[q^2-(q_t^2+m^2/2)]^2}. \tag{13}$$

$m$ denotes the mass of the propagating particle, $q$ is its four-momentum, and $q_t^2$ is the value of $q^2$ at the kinematical threshold in the $t$ channel. All parametrizations fulfill the following criteria: (i) they are only functions of $q^2$, (ii) they have no pole on the real axis, and (iii) $F(m^2)=1$.

Furthermore, $F_p$ and $F_e$ have a maximum at $q^2=m^2$. $F_p$ resembles a monopole factor $\Lambda^2/(\Lambda^2+\boldsymbol{q}^2)$ in the nonrelativistic limit; this form was also successfully used in other calculations [7,17]. Cloudy-bag models [25], on the other hand, yield form factors $F\sim\exp(-c\boldsymbol{k}^2)$. $F_e$ therefore can be viewed as an extrapolation of this form to other kinematical regimes. The main difference between $F_p$ and $F_e$ is that $F_e$ falls off more rapidly than $F_p$ far away from the resonance position. A comparison of the extracted parameters therefore allows for a study of the influence of the off-shell contributions. In contrast to $F_p$ and $F_e$ the form factor $F_t$ enhances contributions at energies below the resonance positions and does not modify the threshold amplitudes. It was used for $t$-channel exchanges only and was constructed to preserve the connection to the chirally symmetric ansatz of the nonlinear $\sigma$ model.

In general, one would not expect to have the same value for the cutoff $\Lambda$ for all vertices. To take all possibilities into account we would need to perform calculations for all combinations of couplings and form factors, allowing $\Lambda$ to vary independently for each vertex. Since this would introduce too many free parameters, we limit ourselves to the following recipe: (i) the same functional form $F$ and cutoff $\Lambda_N$ are used in all vertices $\pi NN$, $\eta NN$, and $KN\Lambda$, (ii) for all resonances we take the same $F$ as for the nucleon, but different values $\Lambda_{1/2}$ and $\Lambda_{3/2}$ for the cutoffs for spin-$\frac{1}{2}$ and spin-$\frac{3}{2}$ resonances, and (iii) in all $t$-channel diagrams the same $F$ and $\Lambda_t$ are used.

The nucleon is treated differently than the resonances in order to account for its special importance for all reactions. The resonances themselves are split up into two categories according to their spin, since the form of the couplings is mainly determined by the spin of the resonances, as can be seen from Eqs. (10)–(12). To account for the different nature of $t$-channel contributions the functional form of the form factor and the value of the cutoff are chosen independently from $s$ and $u$ channels.

### D. Calculation of the *T* matrix

Once the Lagrangians and form factors are specified, we have to compute the $K$ matrix for all reactions and deduce from this the $T$ matrix with the help of Eq. (8). Here we only sketch this procedure; all formulas needed are collected in Appendix A.

As in $\pi N$ scattering [21], we decompose the invariant matrix element $\mathcal{M}_{fi}$ for mesons with the same parity in the initial and final state as

$$\mathcal{M}_{fi}=\overline{u}(p',s')(A+B\not{Q})u(p,s), \tag{14}$$

with $Q$ being the average of both meson four-momenta: $Q=(q+q')/2$. Since the most general case of the scattering amplitude can be written in terms of Pauli spinors as [26]

$$\mathcal{M}_{fi}=\frac{4\pi\sqrt{s}}{\sqrt{mm'}}\chi_f^\dagger\mathcal{F}\chi_i, \quad \mathcal{F}=\tilde{A}+\tilde{B}\boldsymbol{\sigma}\cdot\hat{\boldsymbol{p}}'\boldsymbol{\sigma}\cdot\hat{\boldsymbol{p}}, \tag{15}$$

with the known partial-wave decomposition

$$\begin{aligned}\mathcal{F}=&\frac{1}{\sqrt{\mathrm{qq}'}}\sum_{l=0}^{\infty}[lT_{l-}+(l+1)T_{l+}]P_l\\&+i\boldsymbol{\sigma}\cdot(\hat{\boldsymbol{p}}\times\hat{\boldsymbol{p}}')[T_{l+}-T_{l-}]P_l',\\ T_{l\pm}=&\frac{\sqrt{\mathrm{qq}'}}{2}\int_{-1}^{1}d\cos\theta\,[\tilde{A}P_l(\cos\theta)+\tilde{B}P_{l\pm}(\cos\theta)],\end{aligned} \tag{16}$$

we can extract the $T_{l\pm}$'s by inserting the explicit representation of the spinors and $\gamma$ matrices [27] into Eq. (14). The resulting expressions for $\tilde{A}$ and $\tilde{B}$ in terms of $A$ and $B$ are slightly more complicated than in $\pi N$ scattering because we also have to take into account that the initial and/or final hadron may not be a nucleon. For reactions involving mesons with different parity the procedure is similar and the results are listed in Appendix A.

Once the partial-wave amplitudes $T_{l\pm}$ are given it is straightforward to extract the various observables using standard formulas (see Appendix B and [26]). To include all contributions to the cross sections we have calculated the partial waves up to $l_{\max}=5$. In this way the convergence of the partial-wave expansion is guaranteed.

## V. RESULTS OF THE FITS

In order to check our numerics, we have reproduced the analytic results of Hachenberger and Pirner [28] for the $\pi N$ amplitude and the results of Deutsch-Sauermann *et al.* [7]. Especially the nonresonant background has to be checked, because sign errors would remain undetected in this case. The contributions of the resonances are easily tested since for the $s$-channel diagrams the $K$ matrix for a given reaction $i\to f$ via a channel with quantum numbers $\alpha$ can be written as

TABLE II. $\chi^2$ values for the different fits. $\chi^2/N_{\rm DF}$ gives the $\chi^2$ per data point. Also the $\chi^2/N_{\rm DF}$ values for the different reaction channels are given separately.

| | $\chi^2$ | $\chi^2/N_{\rm DF}$ | $\chi^2_\pi/N_{\rm DF}$ | $\chi^2_{\pi\pi}/N_{\rm DF}$ | $\chi^2_\eta/N_{\rm DF}$ | $\chi^2_K/N_{\rm DF}$ |
|---|---|---|---|---|---|---|
| KA84-pp | 4196 | 2.84 | 2.50 | 6.52 | 1.42 | 3.14 |
| KA84-ee | 4616 | 3.13 | 2.99 | 5.59 | 1.58 | 3.52 |
| KA84-pt | 4067 | 2.76 | 2.41 | 5.70 | 1.50 | 3.39 |
| SM95-pp | 4720 | 3.62 | 3.78 | 6.27 | 1.49 | 3.31 |
| SM95-ee | 4871 | 3.74 | 4.11 | 5.60 | 1.61 | 3.28 |
| SM95-pt | 4574 | 3.52 | 3.69 | 5.67 | 1.64 | 3.22 |

$$K^\alpha_{fi}=\frac{-m_R\sqrt{\Gamma^\alpha_f(s)\Gamma^\alpha_i(s)}}{s-m^2_R}, \tag{17}$$

which has a pole at the resonance mass. Therefore a cancellation of divergent $K$-matrix elements occurs when computing the $T$ matrix with the help of Eq. (8). Any error in the computation of the $K^\alpha_{fi}$'s would show up as a pole in $T^\alpha$. The signs of the couplings can anyway only be determined relative to the other contributions to the same reaction.

The $\chi^2$ fits were performed using the Levenberg-Marquardt algorithm. The code was derived from the IMSL routine ZXSSQ and checked against the original version. For a number of random parameter sets the local minimum was determined and the best of them was taken to be the global minimum. In general the parameters have been allowed to vary in the ranges given by the Particle Data Group [8]. For the off-shell parameters the allowed range was set to $-2 \leqslant 1/2(1+2z) \leqslant 2$. To further verify the final parameter sets they were also used as starting points for a global minimization employing two other algorithms.

We extracted six parameter sets in total, using three different form factors at the vertices for each of the two $\pi N$ PWA's: (i) $F_p$ for the coupling of nucleon, resonances, and $t$-channel exchanges, (ii) $F_e$ for the coupling of nucleon, resonances, and $t$-channel exchanges, and (iii) $F_p$ for the coupling of nucleon and resonances, $F_t$ for $t$-channel exchanges.

In the following the notation is such that KA84 [2] or SM95 [4] denote the $\pi N$ data used in the fits. Two additional letters indicate the choice of form factors for $s$- and $t$-channel contributions. Thus, for example, SM95-pt denotes a fit to the SM95 PWA with $F_p(q^2)$ used for the vertices of propagating hadrons and $F_t(q^2)$ for the $t$-channel diagrams.

Looking at the $\chi^2$ values of the fits as given in Table II, it seems at first glance that the use of the KA84 PWA leads to better overall fits. This, however, is mainly due to the fact that the *single-energy* values of SM95 scatter around the energy-dependent solution. That the fits for KA84 and SM95 are indeed of equal quality can be seen from the figures and also from the very similar values of $\chi^2/N_{\rm DF}$ for channels other than $\pi N$ (Table II).

The scattering lengths and effective ranges we find are in general agreement with the values obtained by other groups. This can be seen from Table III, where we list both parameters $a_I$ and $r_I$ extracted from the phase shift $S_{1I}$ close to threshold [26]:

TABLE III. $\pi N$-, $\eta N$-, and $K\Lambda$-scattering lengths as obtained in the fits in comparison with the results of other works. The number in brackets indicates the error in the last digits.

| | | KA84-pp [fm] | SM95-pt [fm] | Others [fm] |
|---|---|---|---|---|
| $\pi N$ | $a_1$ | 0.180 | 0.168 | 0.247, [a] 0.246, [b] 0.252 [c] |
| | $r_1$ | $-2.430$ | $-3.062$ | – |
| | $a_3$ | $-0.114$ | $-0.142$ | $-0.144$, [a] $-0.130$, [b] $-0.143$ [c] |
| | $r_3$ | 13.300 | 7.668 | – |
| $\eta N$ | $a_1$ | $0.487 + i0.171$ | $0.577 + i0.216$ | $0.51 + i0.21$ [d] |
| | | | | $0.717(30) + i0.263(25)$ [e] |
| | | | | $0.751(43) + i0.274(28)$ [f] |
| | $r_1$ | $-6.060 - i0.177$ | $-2.807 - i0.057$ | $-1.496(134) - i0.237(37)$ [f] |
| $K\Lambda$ | $a_1$ | $0.065 + i0.040$ | $0.048 + i0.030$ | – |
| | $r_1$ | $-15.930 - i8.252$ | $-24.324 - i13.853$ | – |

[a]Reference [21].
[b]Reference [4].
[c]Reference [2].
[d]Reference [7].
[e]Reference [6].
[f]Reference [29].

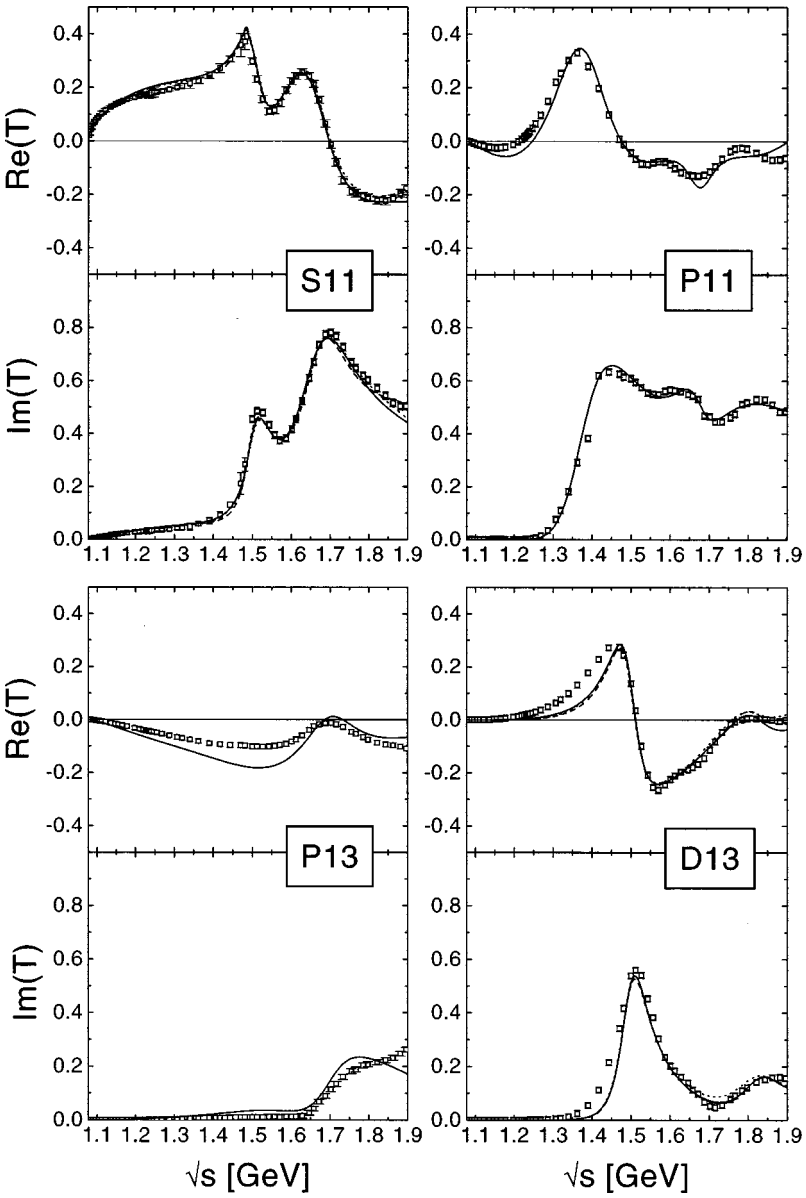


FIG. 1. Fits to the $\pi N$ $I=\frac{1}{2}$ partial waves from KA84 [2]. Fits KA84-pt (solid line), KA84-pp (dashed line), KA84-ee (dotted line) (the latter two are only shown for $S_{11}$ and $D_{13}$). For the notation used in labeling the fits see Sec. V.

$$|\boldsymbol{q}|\left(\frac{1}{S_{1I}}+i\right)\approx\frac{1}{a_I}+\frac{1}{2}r_I|\boldsymbol{q}^2|. \tag{18}$$

Here $\boldsymbol{q}$ denotes the meson three-momentum. The deviations from the known $\pi N$ values are due to the fact that we fit the data over the whole energy range and do not put special emphasis on the threshold region. Since the Born terms and the $\rho$ contribution dominate both the threshold amplitudes and the nonresonant background, the high-energy behavior of these terms also influences the $\pi N$-scattering length. This will be discussed in detail in Sec. VI A. In the $\eta N$ channel we find a smaller scattering length but a larger effective range. This indicates that in our model the $S_{11}$ partial wave does not rise as steeply as in other models [6,29].

In order to compare the different fits in detail, we will first look at the different reaction channels and then discuss the parameters found.

### A. $\pi N \to \pi N$

For the fits using both the KA84 and SM95 PWA all form factors lead to a comparably good description of the data (Figs. 1–4). We only show the results for the channels $S_{11}$, $D_{13}$, and $P_{33}$ since in the other channels the difference is even smaller. All structures present in the data are well reproduced. From this we conclude that all major resonances relevant in this energy range were taken into account. The only exception seems to be the $P_{31}$ channel. The data clearly show the contribution of a resonance with a mass of 1.9–2.0 GeV. Since a reliable determination of its parameters is not possible from the fit to the lower-energy part of the resonance only, we fit this channel only up to 1.6 GeV. A similar situation is encountered in the $S_{31}$ channel where the maximum energy fitted was 1.8 GeV. In principle, higher-lying resonances could contribute to all partial waves; therefore it is clear that the fits might not reproduce the data for energies $> 1.8$ GeV.

As a general tendency, the fits seem to be better in the $S_{I1}$ and $P_{I1}$ channels than in $P_{I3}$ and $D_{I3}$. This might indicate a shortcoming in the description of spin-$\frac{3}{2}$ resonances. Either the use of a common shape for the form factor for spin $\frac{1}{2}$ and spin $\frac{3}{2}$ is too restrictive or we are missing contributions from resonances with spin $>\frac{3}{2}$. As can be seen from Fig. 5, the

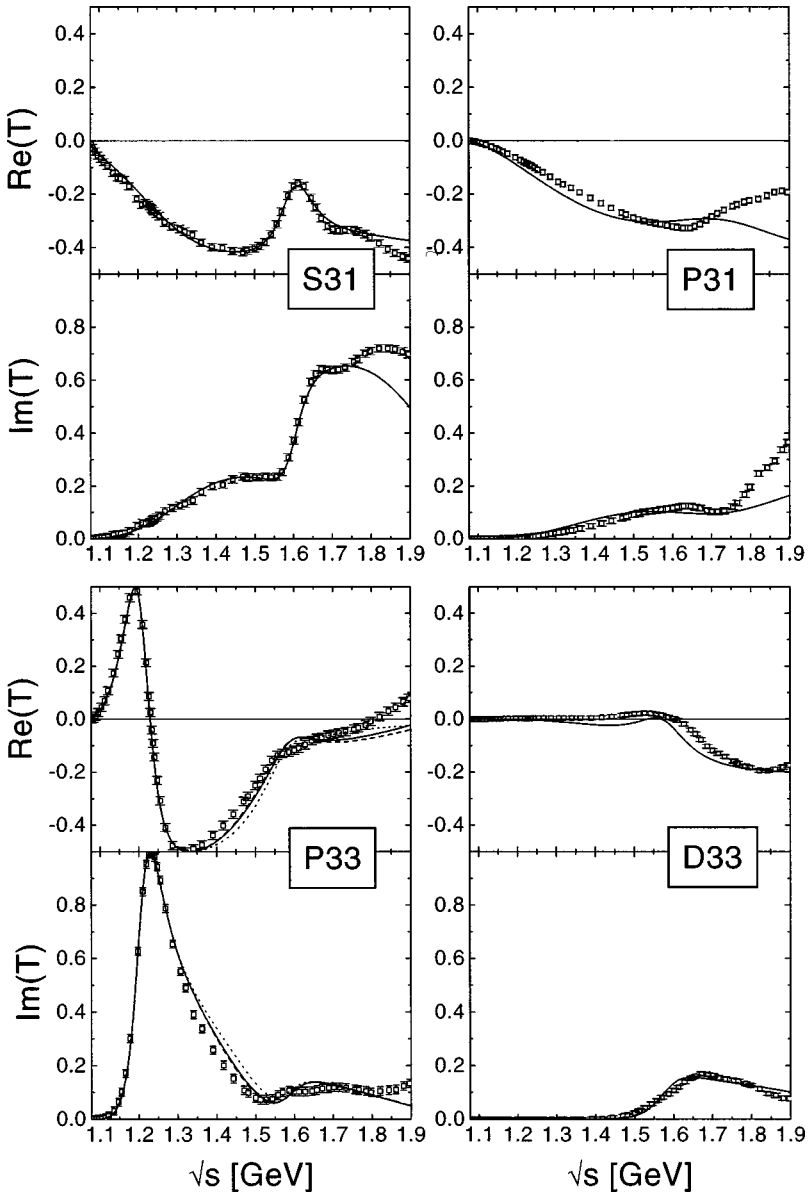


FIG. 2. Results for the $I=\frac{3}{2}$ channels. Legend as in Fig. 1. Here KA84-pp and KA84-ee are shown for $P_{33}$ only.

spin-$\frac{3}{2}$ resonances contribute sizably to spin-$\frac{1}{2}$ channels away from their mass shell. These contributions depend on the value of the $z$ parameters from Eqs. (12), but cannot be completely suppressed. In turn, the same might be true for resonances with higher spin. At this point we cannot safely distinguish between the two explanations.

It is interesting to note the systematics of the deviations from the data: below a resonance it seems that we underestimate the resonance contribution [e.g., $D_{13}(1520)$, Fig. 1], whereas for energies above the resonance position the contribution does not fall off quickly enough [e.g., $P_{33}(1232)$, Fig. 2]. This might indicate that a form factor that is asymmetric around the resonance position might lead to a better description of the data. Such a parametrization would then be closer to the widely used form factors that depend on the meson three-momentum $\boldsymbol{q}$:

$$F_q=\left(\frac{\Lambda^2+\boldsymbol{q}_R^2}{\Lambda^2+\boldsymbol{q}^2}\right)^{\alpha}. \tag{19}$$

First tests with a possible generalization of Eq. (19) show that this is indeed the case and that the parameters of the spin-$\frac{3}{2}$ resonances might be extracted more reliably using an asymmetric form factor.

In summary, we find, that we can reproduce both PWAs equally well within our model. The small differences between them (e.g., in the $S_{11}$ channel for energies $\approx$ 1.55 GeV) lead to slightly different resonance parameters, but the resulting systematic error is smaller than the uncertainty coming from the different form factors used.

### B. $\pi N \to \pi\pi N$

Not surprisingly, the $\chi^2$ values we find for the different reactions (Table II) clearly show that the $\pi N \to \pi\pi N$ channel gives the largest contribution to the total $\chi^2$. Nevertheless, it is important to check for unusual discrepancies in specific partial waves, because these might indicate that resonances are missing in our calculation.

Despite the simple approximation of the two-pion state by an effective $\zeta$ meson we find overall good fits to the partial cross sections (Figs. 6 and 7). This confirms that the main

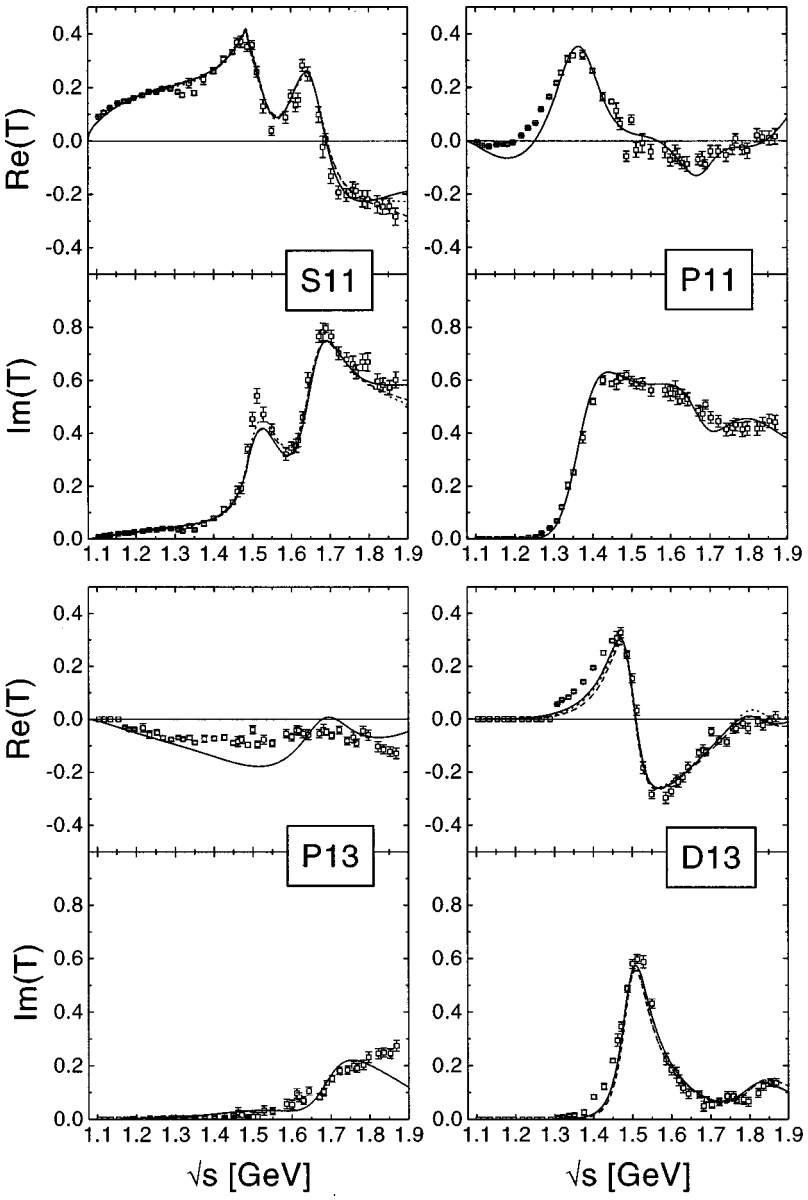


FIG. 3. Fits to the $\pi N$ $I=\frac{1}{2}$ partial waves from SM95 [4]. Fits SM95-pt (solid line), SM95-pp (dashed line), and SM95-ee (dotted line) (the latter two are only shown for $S_{11}$ and $D_{13}$). For the notation used in labeling the fits see Sec. V.

source of inelasticity is taken into account properly.

An exception to this is the $P_{13}$ channel, where we are not able to reproduce the $\pi N \to \pi\pi N$ data at all. According to Manley and Saleski the cross section opens up at about 1.7 GeV, but the inelasticity (as deduced from the $\pi N$ scattering) is much larger already for energies below 1.7 GeV. Since this is the only resonance showing such a behavior, we choose not to introduce a new reaction channel, but to fit the $P_{13}$ parameters disregarding the $\pi\pi N$ data. The coupling of the $P_{13}(1720)$ resonance to $\pi\pi N$ is therefore determined by the inelasticity in the $\pi N$ channel alone. It is thus remarkable that the calculated $\pi N \to \zeta N$ cross section exhausts all of the inelastic cross section, at least up to $\approx$ 1.75 GeV.

A large inelastic cross section (as deduced from the KA84/SM95 data) could in principle also stem from decays into other final states. However, $\eta N$ or $K\Lambda$ is ruled out, because in this case we would not be able to fit the corresponding data for $\pi^- p \to \eta n$ and $\pi^- p \to K^0\Lambda$. Manley and Saleski indeed assumed a coupling of a second $P_{13}$ resonance $[P_{13}(1879)]$ to the $\omega N$ channel to account for a $3\pi$ decay. The choice of this additional channel is, however, arbitrary, since in principle also other decays (e.g., $\rho\Delta$) could also contribute.

There are unfortunately already differences between the inelastic cross sections (defined in Appendix B) as determined from KA84 on the one hand and the $\pi N \to \pi\pi N$ data as given by Manley and Saleski (e.g., in the $S_{31}$ and $D_{33}$ channels) on the other hand. Especially for the $I=\frac{3}{2}$ channels this is clearly a model-independent problem in the data analyses, since there is no other decay channel than $\pi\pi N$ in the energy range up to 1.6 GeV.

### C. $\pi^- p \to \eta n$

All parameter sets give similar fits to the total and differential cross sections (see Figs. 8 and 9) and the partial waves[3] (Fig. 10). Above 1.65 GeV we find that we cannot fully reproduce the falloff in the forward direction (Fig. 7).

[3]To avoid confusion we plot $T^{1/2}_{\pi\eta}$ and $T^{1/2}_{\pi K}$ in the usual notation $\langle b|T_{ba}|a_i\rangle = \tau_i T^{1/2}_{ba}$ [21] instead of the one given in Appendix A.

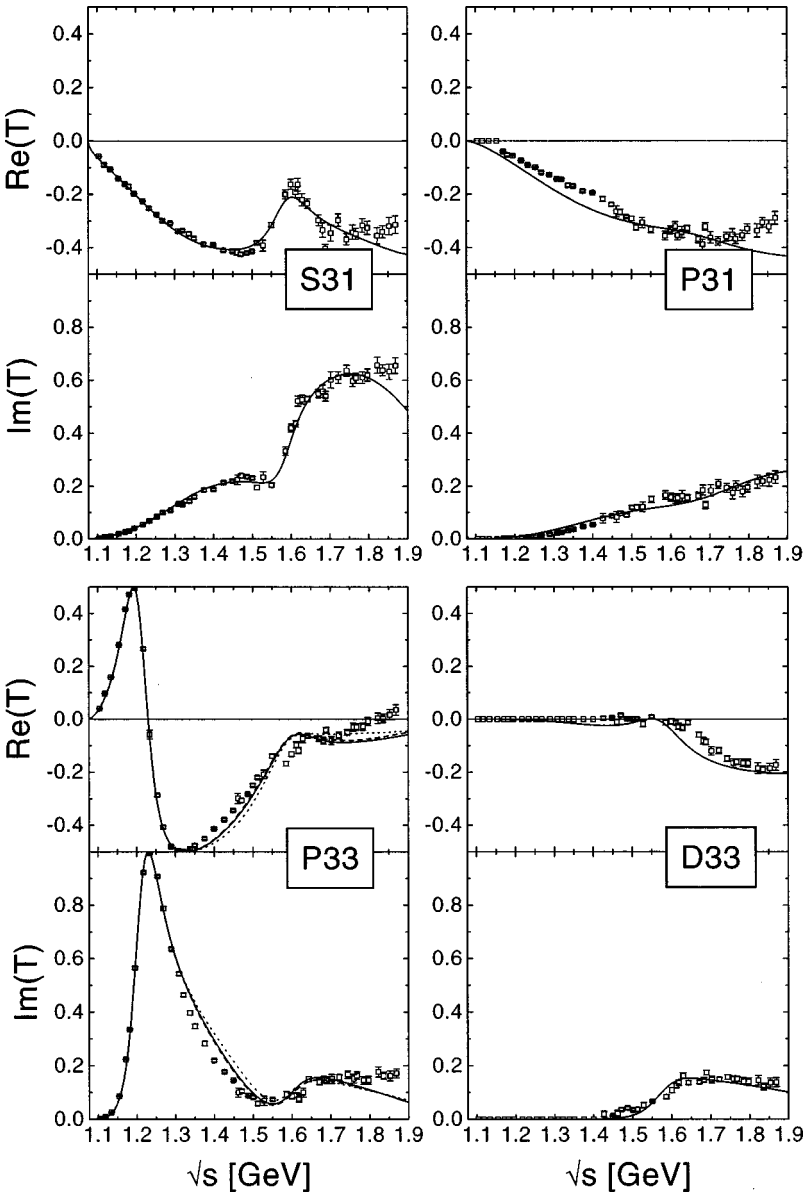


FIG. 4. Results for the $I=\frac{3}{2}$ channels. Legend as in Fig. 3. Here SM95-pp and SM95-ee are shown for $P_{33}$ only.

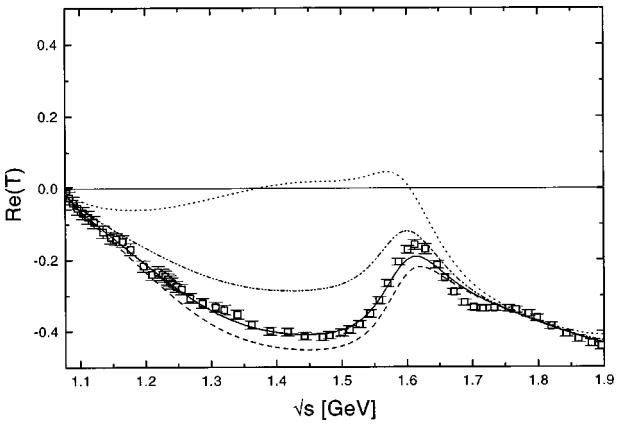


FIG. 5. Influence of the $z_\pi$ parameter of the $P_{33}(1232)$ on the $S_{31}$-phase shift. KA84-pt (solid line), $z_\pi=-0.5$ (dashed line), $z_\pi=0.0$ (dot-dashed line), and no $P_{33}(1232)$ (dotted line).

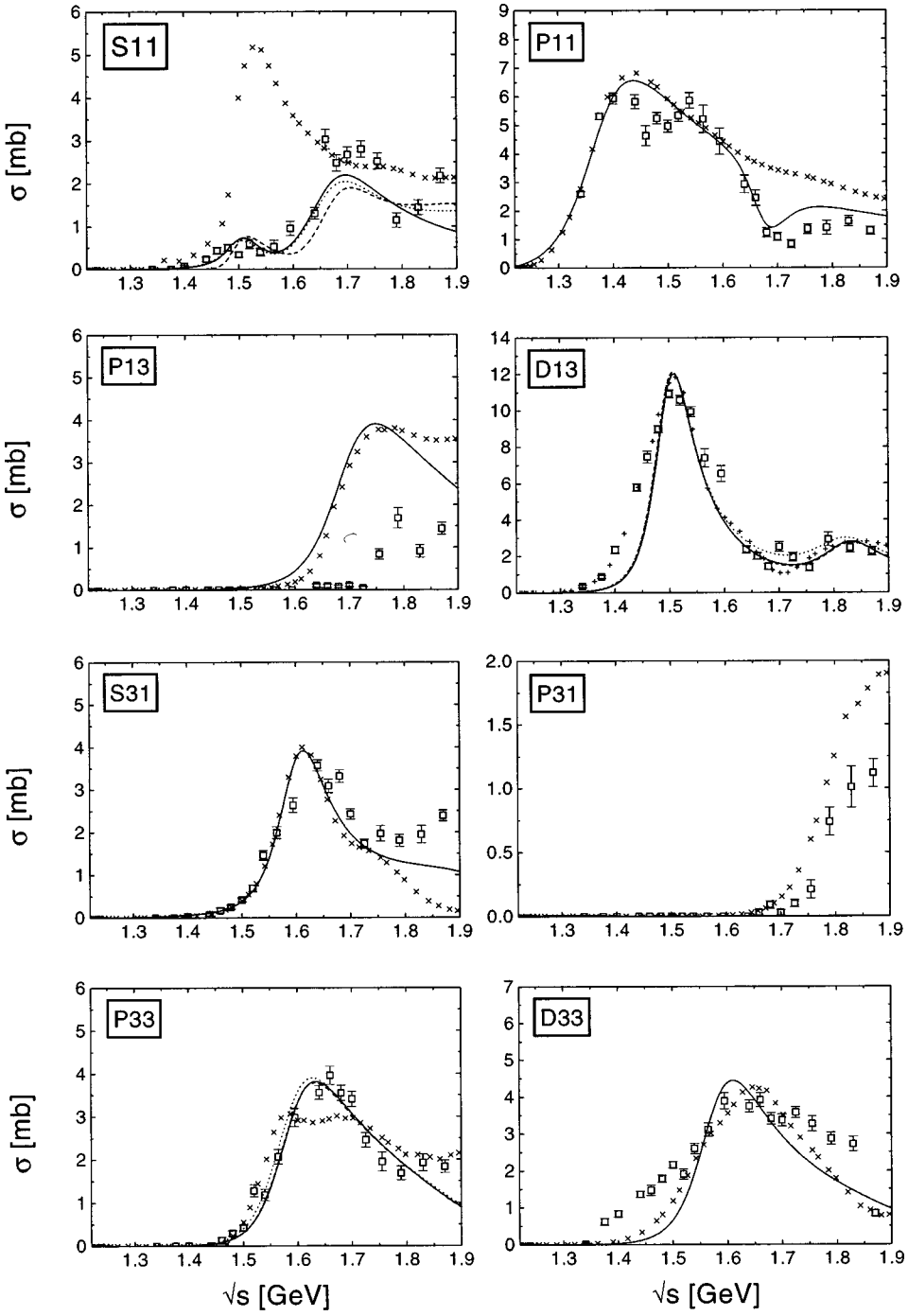


FIG. 6. Comparison of the calculated $\pi N \to \pi\pi N$ cross sections for the fits using the KA84-PWA with data from [3]. Legend as in Fig. 1. In addition the inelastic cross section ($\times$) as determined from the KA84 PWA is shown [cf. Eq. (B4)].

Batinić *et al.* [6] were able to describe the differential data over the whole energy range, by requiring additional $S_{11}$ and $P_{11}$ resonances with a sizable $\eta N$ coupling. Unfortunately, most of the data at higher energies are from Brown *et al.* [30], which show the largest uncertainties. Despite this fact the $\pi^- p \to \eta n$ reaction might be a suitable channel to search for resonances with a weak coupling to $\pi N$. To investigate this in detail, we would have to enlarge the energy range of our fits to be able to extract parameters for resonances with masses of 1.9–2.0 GeV reliably. With five to six resonances coupling to the $\eta N$ channel, better differential data and also polarization observables would be needed, to disentangle their contributions safely.

The agreement between the different fits in the calculated partial waves is quite good. The discrepancies in the $P_{11}$ channel are readily explained by small changes in the nearly vanishing coupling of the $P_{11}(1710)$ to the $\pi N$ channel. Because of the smallness of this coupling, the fits easily differ by 100% for its absolute value.

That the available data (especially with the weights given by Batinić *et al.*) do not put too strong constraints on the $\eta N$ couplings can be seen best when looking at the total cross sections (Fig. 8). Even though they show sizable deviations from each other above 1.65 GeV, all of them lead to rather similar $\chi^2$ values in this channel.

### D. $\pi^- p \to K^0 \Lambda$

As in the case of $\pi^- p \to \eta n$ inconsistencies between different measurements of the cross sections can be observed

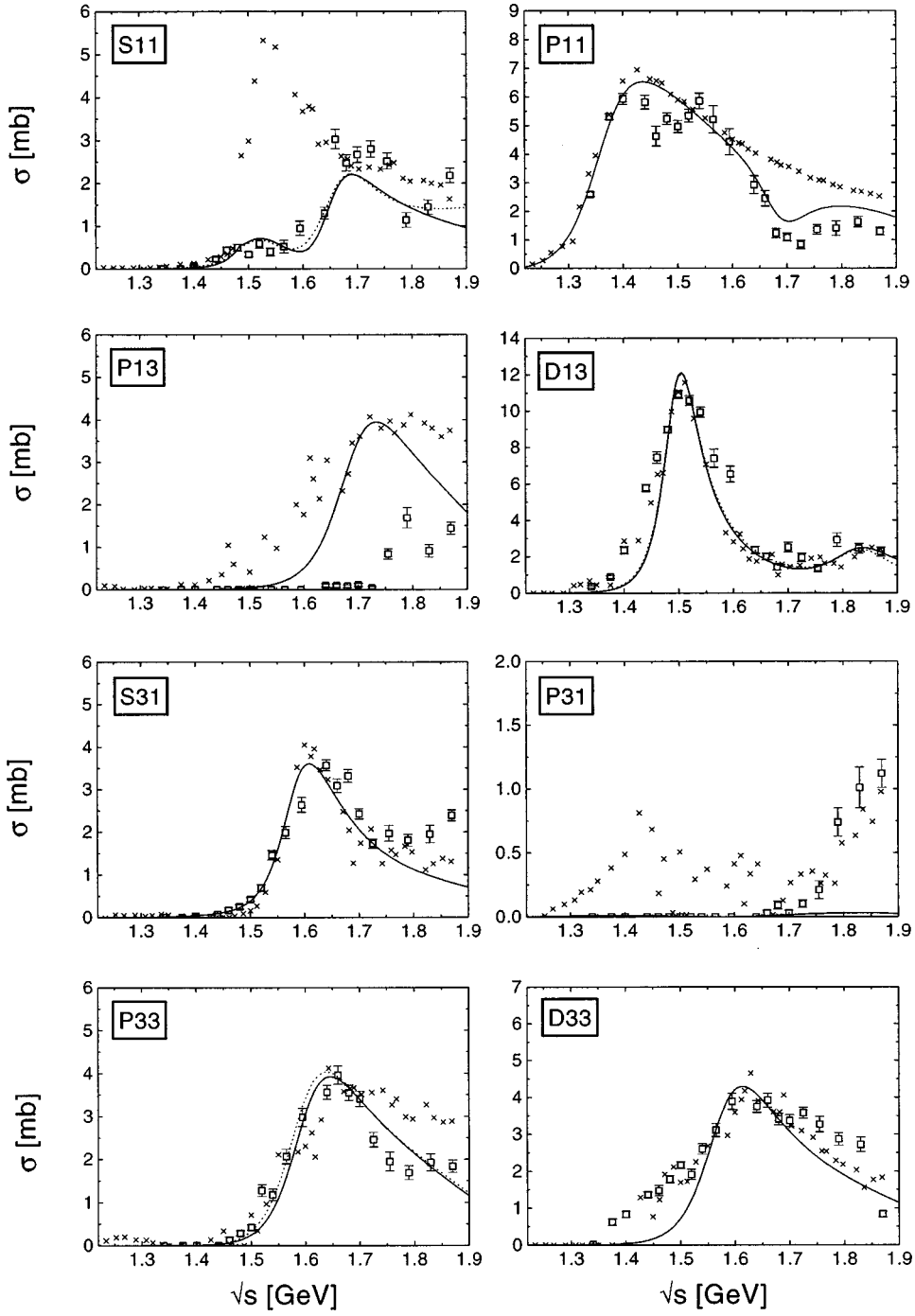


FIG. 7. Comparison of the calculated $\pi N \to \pi\pi N$ cross sections for the fits using the SM95 PWA with the data from 3. Legend as in Fig. 3. In addition the inelastic cross section ($\times$) as determined from the SM95 PWA is shown [cf. Eq. (B4)].

(e.g., at 1.694 GeV in Fig. 11). Besides, the errors of the polarization data given in [31] are extremely large. In practice these data do not constrain the couplings at all. So better data are needed also in this channel. The contribution of this channel to the total $\chi^2$ is larger than the one from $\eta$ production (Table II). This is mainly due to the fact that we enlarged the errors in the case of $\pi^- p \to \eta n$.

In Fig. 12 we show the partial waves extracted from our calculations together with the results of Sotona and Žofka [20], obtained from an analysis of $\pi^- p \to K^0 \Lambda$ only. Since we find an appreciable coupling to the $K\Lambda$ channel only for two resonances [$S_{11}(1650)$ and $P_{11}(1710)$], all our fits yield very similar partial waves. In contrast to this, the values from Sotona and Žofka differ strongly from our results. Nevertheless, for energies below 1.8 GeV both models describe the experimental data equally well. This shows the importance of coupled channel analyses, since the data for the $\pi^- p \to K^0 \Lambda$ reaction alone obviously are not sufficient to determine the partial waves (and thus the resonance parameters) uniquely.

We again stress that we do not include all contributions to $\pi^- p \to K\Lambda$ in our analysis. As already pointed out in Sec. II, hyperon resonances are omitted and therefore $u$-channel contributions are missing in our calculation. Furthermore, rescattering through a $K\Sigma$ intermediate state might change the angular distribution. The influence of this additional channel

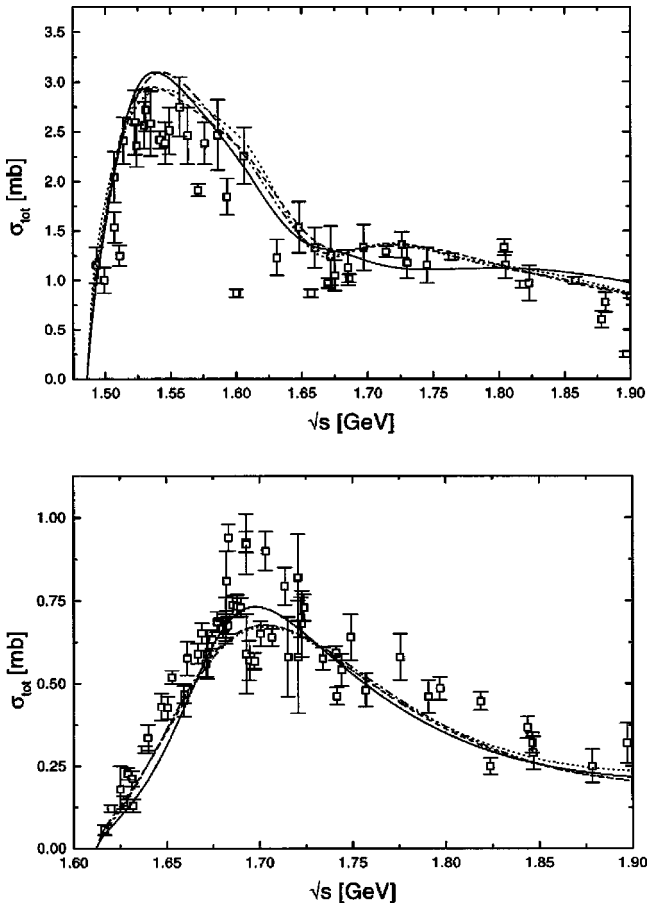


FIG. 8. Results for the total $\pi^- p \to \eta n$ (upper plot) and $\pi^- p \to K^0 \Lambda$ (lower) cross sections. Shown are the fits KA84-pt (solid line), KA84-pp (dashed line), SM95-pt (dot-dashed line) and SM95-pp (dotted line). Data as in Figs. 9 and 11.

can be seen in Fig. 13, where we also show the results of Kaiser *et al.* [12] for the total $\pi^- p \to K^0 \Lambda$ cross section. In their calculation the cusp due to the opening of the $K\Sigma$ channel at 1.68 GeV is clearly visible.

Keeping this in mind we find that the fits account for most of the data. Only for the highest energies considered there are indications for additional contributions from resonances omitted here (see Fig. 14, right). For the good overall quality of the fit the $K^*$ meson is essential, as can be seen from Fig. 14. For higher energies the forward peak is solely due to this $t$-channel contribution. At the same time, the influence on the cross section at other angles is small so that the resonance couplings can still be determined quite accurately.

## VI. PARAMETERS AND COUPLINGS

From the detailed discussion in the last section it is evident that a simultaneous description of all available data is possible within the present model. The most important resonances and the dynamical rescattering seem to be incorporated correctly; therefore reliable parameter estimates are possible. Thus, we now turn to the discussion of the couplings found in the various fits, starting with the background parameters. As already pointed out, the nonresonant background results from only a few Feynman diagrams, and therefore cannot be varied independently for each channel. As a consequence the extraction of the resonance parameters depends strongly on the quality of the ''overall fit.'' This will be made clear in more detail at the end of this section.

In general we find that the systematical error that can be deduced from fits with different form factors and/or data sets is more important than the statistical error found in each fit. We therefore do not give any statistical errors for the parameters in the various tables.

### A. Meson nucleon couplings

The couplings of the mesons to the nucleon, as determined in the fits, are listed in Tables IV and V. To show the influence of the form factor of the nucleon and the $t$-channel exchanges, we show both the couplings at the on-shell point $\sqrt{s}=m_N$ and at the thresholds of the $s$ and $t$ channels, respectively (Table V). Furthermore, we list the cutoffs $\lambda_{N,1/2,3/2,t}$ in Table VI.

For the couplings to $\pi$, $\eta$, and $K$ (a $\zeta NN$ vertex was not taken into account) we find in general that our values are somewhat smaller than those obtained by other groups. Furthermore, we observe only a small spreading of the values for $g_{\pi NN}$ from the different fits, which indicates the important role of the Born terms for the $\pi N$ nonresonant background. For the other couplings ($g_{\eta NN}$ and $g_{KN\Lambda}$) this is not the case, mainly because the form factors $F_{p,e}$ lead to a large reduction of these contributions ($F_{p,e} \approx 0.3$–$0.7$ at threshold). Even with the couplings $g_{\eta NN}$ and $g_{KN\Lambda}$ set to zero, we would still be able to find a fit to the $\pi N \to \eta N$ and $\pi N \to K\Lambda$ data with only a minor increase of $\chi^2$. This indicates that these processes are determined by $t$-channel and resonance excitations. In meson photoproduction the situation is different, because the requirement of gauge invariance counteracts the influence of the form factor [7,32]. One might therefore be able to extract the $g_{\eta NN}$ and $g_{KN\Lambda}$ couplings more reliably from photoproduction.

Since the nonresonant background in this model contains the Born terms and the $t$-channel exchanges, it is completely determined by a relatively small number of parameters. In particular it cannot be varied independently in different partial waves, as was possible, for example, in [3,6,33]. Therefore, constraints on the background found in one channel might influence parameters extracted from other channels. This provides a stringent test of the model that was not possible in other works.

To illustrate the interplay between background and resonance parameters we look at the $t$-channel contribution of the $\rho$ meson to $\pi N$ scattering. The $\rho$ exchange leads to the following amplitudes [34]:

$$\mathcal{M}_{fi} = \bar{u}(p',s')(A + B\not{Q})u(p,s),$$

$$A = \frac{g_{\rho NN}\kappa_{\rho NN} g_{\rho\pi\pi}}{2m_N} \frac{s-u}{t-m_\rho^2} F(t),$$

$$B = 2g_{\rho NN}(1+\kappa_{\rho NN}) g_{\rho\pi\pi} \frac{1}{t-m_\rho^2} F(t). \qquad (20)$$

Since $(s-u)/(t-m_\rho^2)$ diverges with increasing energy, this contribution will dominate $\pi N \to \pi N$ at high energies. Con-

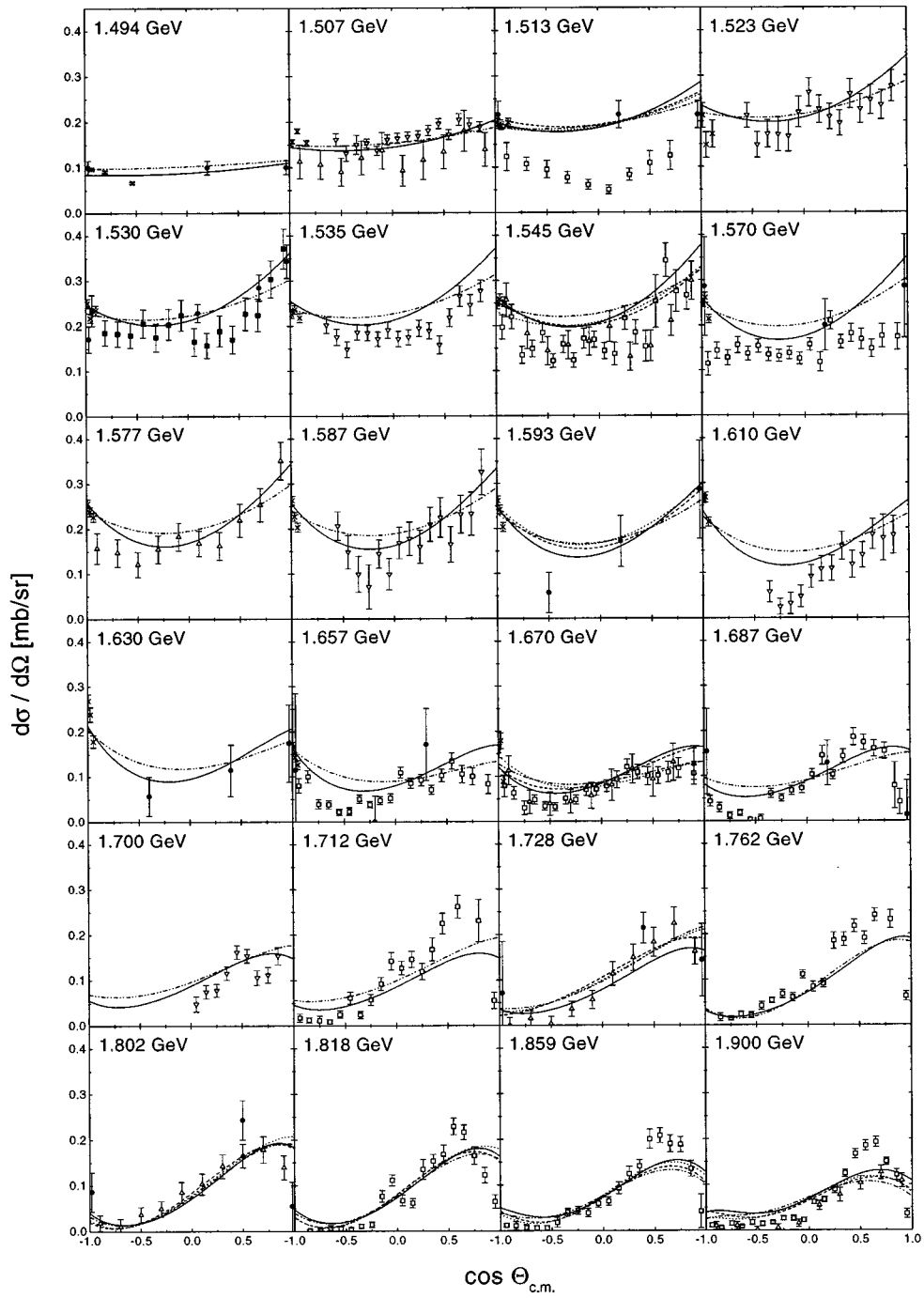


FIG. 9. Comparison with data for the calculated differential $\pi^- p \to \eta n$ cross sections for different energies. Shown are the fits KA84-pt (solid line), KA84-pp (dashed line), SM95-pt (dot-dashed line), and SM95-pp (dotted line). The data points are taken from [41] (●), [42] (×), [43] (▽), [44] (△), [30] (□), and [45] (■).

sequently, the fits try to suppress this divergence by decreasing $g_{\rho NN}$, thus also changing the $\rho$ contribution at low energies.

This effect can be seen best for $\rho$ and $K^*$. With small couplings $g_{\rho NN}$ and $g_{K^*N\Lambda}$ the fit can be improved for the highest energies under consideration, but at the same time the background is too small at lower energies. As a consequence we find systematic deviations for example in the $P_{33}$ channel at about 1.4 GeV (cf. Figs. 2 and 4). This in turn leads to small values for mass and width of the $\Delta$ resonance. From this it is clear that we need a stronger modification of the $\rho$ and $K^*$ contributions even for energies below 2.0 GeV to have the desired Regge-like behavior (e.g., as in [1]). This could possibly be achieved by using a form factor that is a function of all three variables $s$, $u$, and $t$. Such a behavior can at best be approximated by our choices for $F_p$, $F_e$, and $F_t$. For the $a_0$ the situation is less clear, since it is a scalar meson and does not give a divergent contribution to the scattering amplitude.

The values for the tensor coupling of the $\rho$ (Table V) are smaller than the vector-meson dominance (VMD) value of 3.71 used by Höhler and Pietarinen [34], whereas Pearce and Jennings [17] deduced a value of 2.25 in a model similar to ours. It should be noted that in [34] two different form factors have been used for the vector and tensor coupling of the $\rho$. Because of this additional $t$ dependence, it is not straightforward to compare the value given there to ours. Furthermore, one has to keep in mind that Höhler and Pietarinen

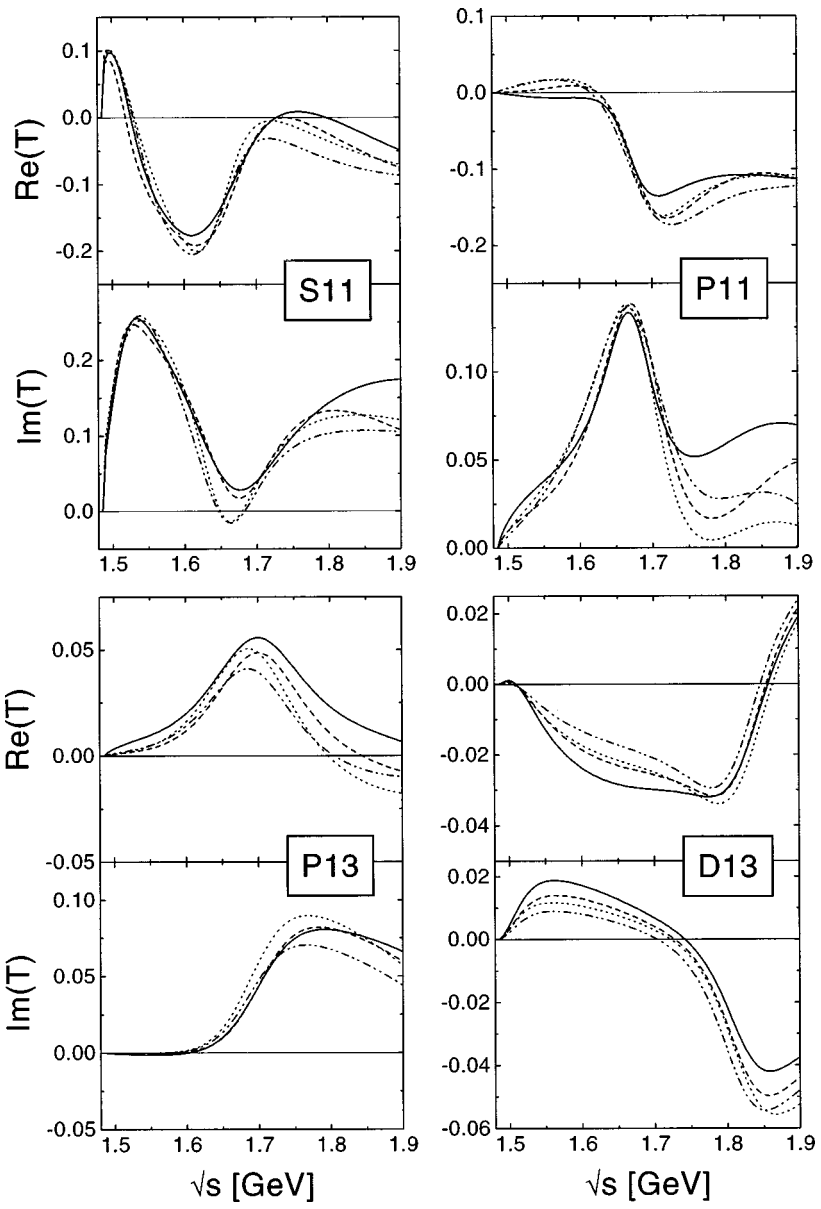


FIG. 10. Calculated partial waves $T^{1/2}_{\pi\eta}$. Legend as in Fig. 9.

used an analytic continuation of the $\pi N$ amplitudes together with the $P$-wave $\pi\pi N\overline{N}$ phase shifts in order to extract the $\rho NN$ vector and tensor couplings. One would therefore expect to find similar values only if dispersion relation constraints would be incorporated in our ansatz. This is clearly one of the main points to improve in further calculations.

For the $K^*$ the tensor couplings are essentially equal in all fits because of the extreme sensitivity of the differential $\pi^- p \to K^0\Lambda$ cross section in the forward direction. This is shown in Fig. 14, where for two energies the $K^*$-meson contribution is turned off. In contrast to this, the coupling of the $a_0$ is not very well determined. This can be traced back to the fact that there are several nucleon resonances with nonvanishing $\eta N$ decays (see Tables VII–XI). Thus, because of the stronger interference of $s$-channel amplitudes, no region exists where the $t$-channel contribution is dominant.

In general all fits yield similar couplings, especially if one focuses on the effective values $g \cdot F$ (see Table V). This indicates that the nonresonant background is properly taken into account apart from the discussed vector-meson contributions at higher energies. Therefore, we expect that the resonance couplings also do not show large deviations between the different fits, since the background is of comparable size.

Unfortunately, we cannot compare our nonresonant contributions to the scattering amplitude to the results of other calculations, since the explicit parameters used for the calculation of the background are usually not given [3,6]. Only Dytman *et al.* [33] show the background for the case of the $S_{11}$ channel. A comparison to our fit KA84-pt is plotted in Fig. 15. One finds drastic differences between both calculations, even though the full amplitude is in good agreement. Especially near threshold our amplitude is dominated by the background, as expected from chiral symmetry [21]. Additionally, in fit KA84-pt one sees the opening of the $\eta N$ threshold even in the nonresonant contribution. This is due to the $D_{13}(1520)$ resonance and its decay into $\eta N$. Both features are not present in the calculation of Dytman *et al.* This shows that a comparison of resonance parameters obtained by groups that use an explicit background parametrization is only meaningful if the background parameters are given.

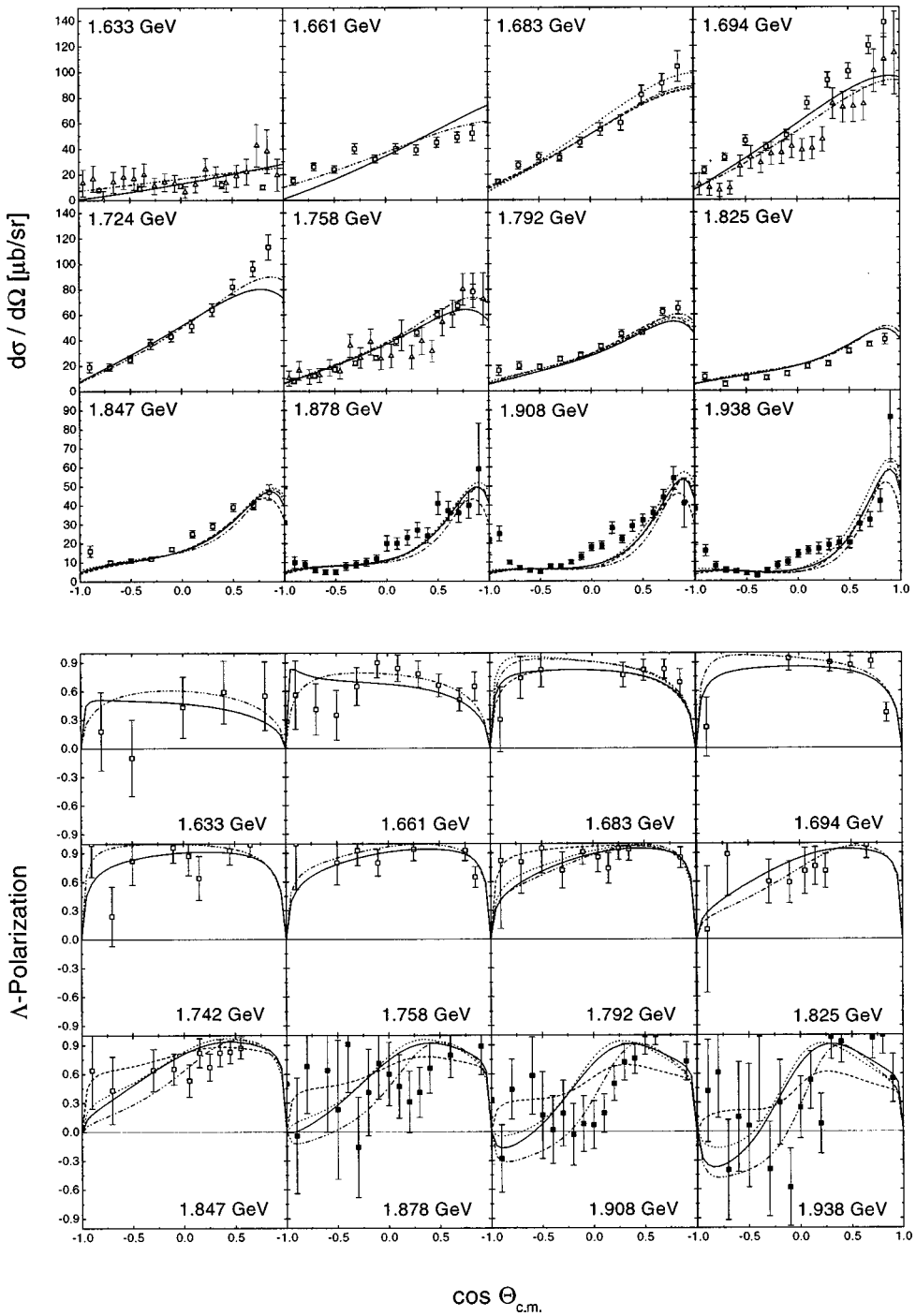


FIG. 11. Comparison with data for the calculated differential $\pi^- p \to K^0 \Lambda$ cross sections and $\Lambda$ polarizations for different energies. Shown are the fits KA84-pt (solid line), KA84-pp (dashed line), SM95-pt (dot-dashed line), and SM95-pp (dotted line). The data points are taken from [46] (□), [47] (△), and [31] (■).

### B. Resonance parameters

In this section we discuss the masses and widths of the nucleon resonances we have extracted. First, the $I=\frac{1}{2}$ resonances in the channels $S_{11}$, $P_{11}$, $P_{13}$, and $D_{13}$, and second, the $I=\frac{3}{2}$ excitations ($S_{31}$, $P_{31}$, $P_{33}$, and $D_{33}$) will be investigated.

For comparison we first quote the results of other analyses in Tables VII–IX. Batinić *et al.* [6] only took $I=\frac{1}{2}$ channels into account and did not include a coupling to $K\Lambda$. In [1], [2], and [4] the $\pi N$-scattering data were used and only the total widths and $\pi N$-branching ratios were given. Manley and Saleski [3] used the data from $\pi N \to \pi N$ and $\pi N \to \pi\pi N$ in their fits; the couplings to other channels were determined from the missing inelasticity only. Therefore, the numbers given for decay channels other than $\pi N$ and $\pi\pi N$ only indicate that additional decay channels are needed to account for the total inelasticity.[4] The different results from the various models illustrate that only the simultaneous fit to all open reaction channels allows the extraction of parameters for resonances with small $\pi N$-branching fraction [e.g., the $P_{33}(1600)$, which was not found in [4]].

In Tables X, XI, and XII we list all masses, decay widths, and $z$ parameters for the six fits done. We do not list the corresponding couplings, since a meaningful comparison to

[4]The only exception is the $S_{11}(1535)$. In this case there is no open channel except $\eta N$ at the resonance energy.

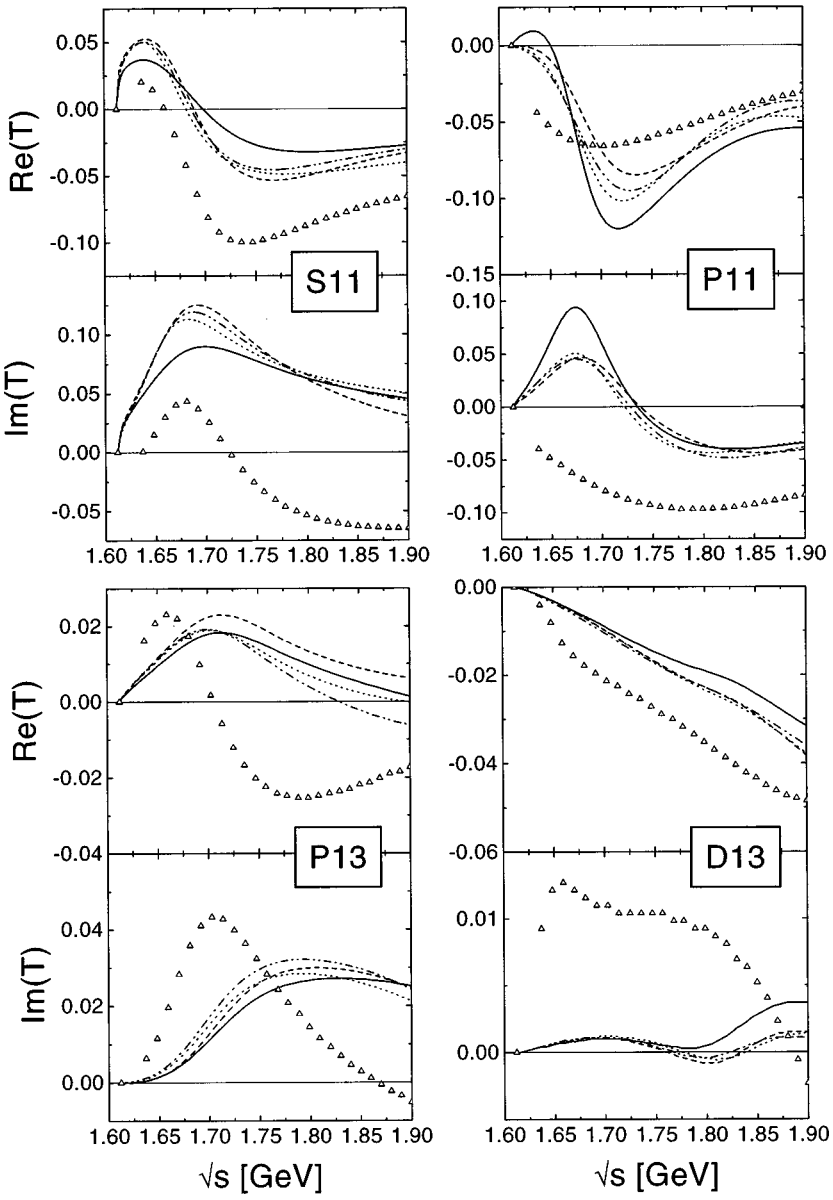


FIG. 12. Calculated partial waves $T_{\pi K}^{1/2}$. Legend as in Fig. 11. In comparison also the results of the calculation of Sotona and Žofka [20] ($\Delta$) are shown.

other calculations can only be done in terms of the decay widths. The reader is referred to Appendix C for a complete list of formulas needed to extract the coupling constants. The decay widths and branching ratios were calculated at the resonance mass ($\sqrt{s}=m_R$); since we include $q$-dependent form factors at the corresponding vertices, the total decay widths do *not* represent the full width at half maximum (FWHM) that is seen, e.g., in the resonance contribution to the total scattering cross section. In brackets we indicate the signs of the coupling constants. These where taken to be the same as in Manley and Saleski [3] for the $\pi N$ and $\pi\pi N$ decays.

#### *1. Isospin-$\frac{1}{2}$ resonances*

*a*. $S_{11}$. For this channel there is a number of detailed models [7,35] that aim to extract the parameters of the $S_{11}(1535)$. It is of special interest because of its large $\eta N$ branching. The deeper reason for this is not well understood and rather different explanations have been given [9–12] (see the corresponding footnote in the Introduction). A reliable value for this parameter would therefore put strong restrictions on all models describing this resonance as an excited state of the nucleon. Since there are at least two resonances in this channel, which are close to each other, a satisfactory fit is only possible if both are included [7]. Furthermore the $s$ waves $S_{11}$ and $S_{31}$ are dominated at threshold by the Born terms and the $\rho$ meson. These contributions therefore determine the scattering lengths. In addition, at least $\pi N\rightarrow\pi N$ and $\pi N\rightarrow\eta N$ have to be taken into account. The reason for that is the large branching fraction of the $S_{11}(1535)$ to both $\pi N$ and $\eta N$ final states. This has two consequences: (i) a reliable determination of the $S_{11}(1535)$ parameters is possible only within a model accounting for all these points and (ii) all extractions are limited by the quality of the $\pi N\rightarrow\eta N$ data.

In Table VII we give in addition the $S_{11}$ parameters extracted from [7,33]. In the work of Deutsch-Sauermann *et al.* the $K$-matrix approach was also used, but within the linear $\sigma$ model instead of the pseudovector $\pi NN$ coupling and without the $\rho$ meson. Despite this difference the agreement of the parameters is quite good; only for the $\eta N$ width do we find some differences (95–113 MeV using KA84 as compared to

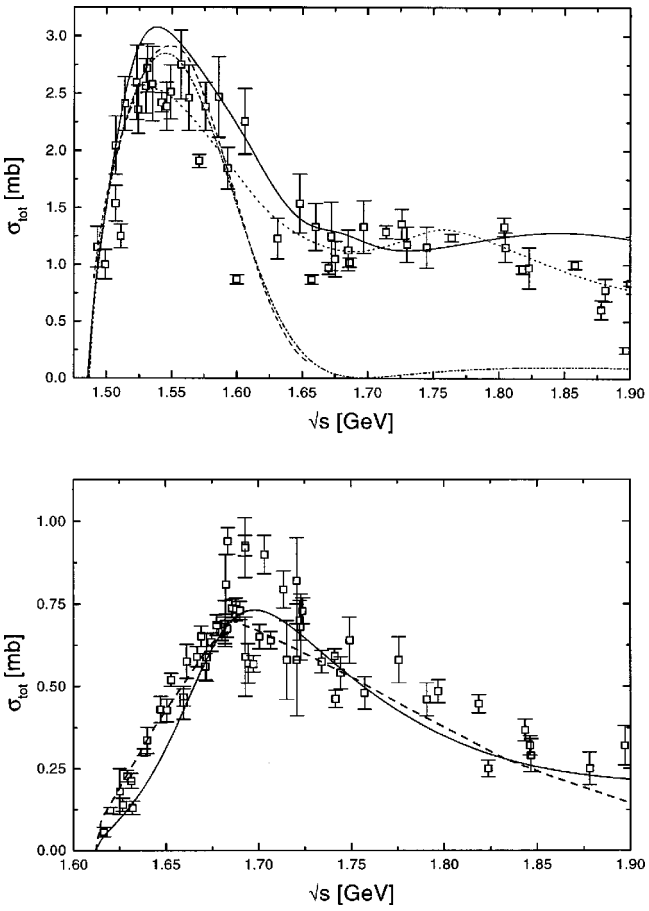


FIG. 13. Comparison of different results for the total $\pi^- p \to \eta n$ (upper plot) and $\pi^- p \to K^0 \Lambda$ (lower) cross sections. Fit KA84-pt (solid line), [12] (dashed line), [7] (dot-dashed line), [6] (dotted line). Data as in Figs. 9 and 11.

89 MeV in [7]) that might be related to the different form factors used. The same holds for the other models as well. As already discussed in the last section, this discrepancy may also be due to the treatment of the nonresonant background in the different calculations.

Unfortunately, the spreading of the parameters is larger for the fits to the SM95 PWA, because we were not able to reproduce the data for the real part of the $S_{11}$ partial wave near the minimum at 1.55 GeV and for the maximum of the imaginary part just above 1.5 GeV (Fig. 3). It is interesting to note that this is also the region of the largest differences of the single-energy data to both the KA84 PWA and the energy-dependent solution of SM95. Maybe the assignment of larger error bars for the $\pi N$ data at these energies would lead to more consistent values for the $S_{11}(1535)$ parameters.

For the second resonance, the $S_{11}(1650)$, a comparable $\pi N$ branching is found in all models, whereas the $\pi\pi N$ width is larger in our fits. Since the $\pi\pi$ states are approximated by a $\zeta$ meson [7], this does not necessarily lead to different scattering amplitudes. Furthermore, we notice that we find no significant coupling of the $S_{11}(1650)$ to the $\eta N$ channel, but a 5–8 % decay into $K\Lambda$. Such a coupling is also known from kaon photoproduction [20,32].

Other models find additional $S_{11}$ resonances at 1.8–1.9 GeV [3,6]. These states might affect the couplings of the $S_{11}(1650)$. Unfortunately, different values are given in the literature for the $S_{11}(2090)$. Therefore, no definite conclusions can be drawn about a possible change of parameters due to this resonance.

*b*. $P_{11}$. Because of the large, energy-dependent background from the Born terms and the $\Delta$ resonance and because of its large decay width, the mass of the $P_{11}(1440)$ cannot be determined very well. Only the branching ratios are in good agreement with the other models (60–70 % $\pi N$, 30–40 % $\pi\pi N$). Again we find that the parameter sets with a higher mass yield larger widths. A coupling to the $\eta N$ channel is found in all fits, but the quality of the data does not allow a precise determination of the $\eta N$ decay width. Since we also have the coupling of the nucleon to the $\eta$, it is questionable if these two contributions can be separated.

In the energy range of the $P_{11}(1710)$ the *t*-channel $\rho$-meson contribution dominates the amplitude. Therefore the parameters of this resonance are sensitive to the form factors and cutoffs used for the $\rho$ and vary accordingly. Interestingly, all fits find a very small ($< 1$ MeV) $\pi N$ coupling so that the contribution to the $P_{11}$ partial wave comes solely from rescattering. Thus the parameters of the $P_{11}(1710)$ are sensitive to the unitarization procedure used in the different models. The structure in the SM95 PWA seems to indicate a much broader resonance in this energy region; we cannot fit these data very well.

*c*. $P_{13}$. All models find that the width of the $P_{13}(1720)$ resonance is dominated by the $\pi\pi N$ decay. The mass we

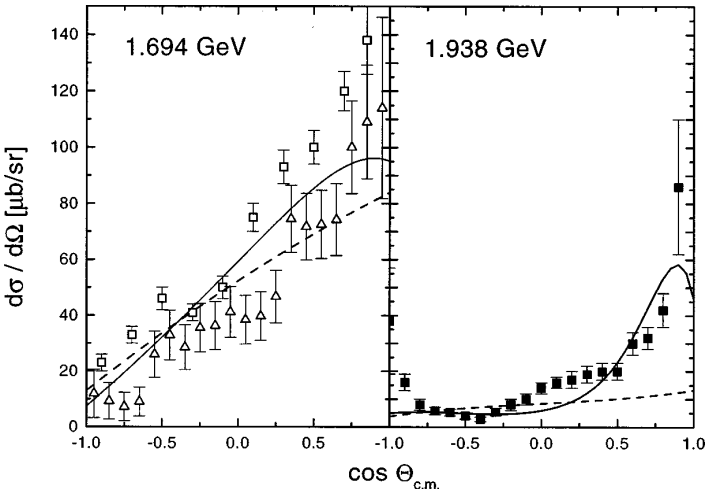


FIG. 14. Importance of the $K^*$-meson contribution to the differential cross section of $\pi^- p \to K^0 \Lambda$ for two different energies. Shown is the calculation using KA84-pt with (solid line) and without (dashed line) the $K^*$.

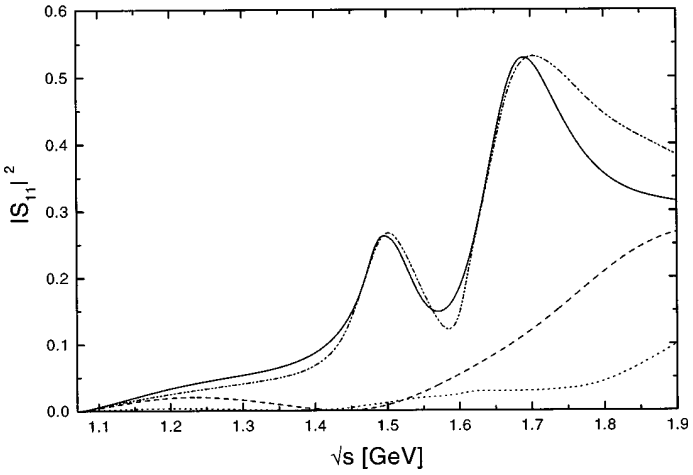


FIG. 15. Comparison with the results from [33]. Plotted is the square of the absolute value of the $S_{11}$-phase shift. Fit KA84-pt (solid line), background only (dashed line), full calculation (dot-dashed line), and background (dotted line) as given by [33].

find in our fits, which is rather high, is determined by the imaginary part of the $\pi N$-phase shift. Since Manley and Saleski [3] list another $P_{13}$ resonance at 1.879 GeV, it is not clear if our $P_{13}(1720)$ is some kind of average of both resonances. To answer this question, the fits would have to be extended to higher energies in order to cover the full range of all possible resonances.

The discrepancies between the inelastic cross section and the $\pi N \to \pi\pi N$ data have been discussed already in Sec. V B; they might be due to a missing decay channel ($\omega N$, $\rho\Delta$). A spread of parameters is also found for the $z$ values, which differ between all fits (see Table XII).

*d*. $D_{13}$. As already mentioned in Sec. V A, we find systematic deviations from the $\pi N$ data for all spin-$\frac{3}{2}$ resonances. Except for the $\Delta$, this effect is most prominent for the $D_{13}(1520)$. The underestimation of the data for energies around 1.4 GeV leads to a small mass in all fits. Related to this we also find smaller values for the partial decay widths, whereas the branching ratios are similar to the values given in Table VIII. Especially the $\eta N$ decay is noticeable. The small width does not imply a small coupling, since the $D_{13}(1520)$ is close to the $\eta N$ threshold at 1.49 GeV. That this coupling can be extracted at all is due to the fact that $s$-wave–$d$-wave interference is responsible for the observed lack of isotropy in the differential $\pi^- p \to \eta N$ cross section around the $S_{11}(1535)$ resonance.

For the $D_{13}(1700)$ the results obtained by other groups vary strongly. Whereas Manley and Saleski [3] give param-

TABLE IV. Couplings of the mesons to the nucleon as obtained in the fits. In the first columns we list the results of the fits KA84-pp, KA84-ee, and KA84-pt, while in the other we give SM95-pp, SM95-ee, and SM95-pt.

| | KA84 | | | | SM95 | | | |
|---|---|---|---|---|---|---|---|---|
| | $g$ | Value | $\kappa$ | Value | $g$ | Value | $\kappa$ | Value |
| $\pi$ | $g_{\pi NN}$ | 13.05 | – | – | $g_{\pi NN}$ | 13.05 | – | – |
| | | 13.06 | – | – | | 13.04 | – | – |
| | | 13.05 | – | – | | 13.05 | – | – |
| $\eta$ | $g_{\eta NN}$ | 1.08 | – | – | $g_{\eta NN}$ | 1.33 | – | – |
| | | 2.39 | – | – | | 0.18 | – | – |
| | | 1.86 | – | – | | 1.13 | – | – |
| $K$ | $g_{KN\Lambda}$ | -6.56 | – | – | $g_{KN\Lambda}$ | -6.36 | – | – |
| | | -6.41 | – | – | | -6.10 | – | – |
| | | -6.06 | – | – | | -6.12 | – | – |
| $\rho$ | $g_{\rho NN}$ | 3.22 | $\kappa_{\rho NN}$ | 2.14 | $g_{\rho NN}$ | 3.37 | $\kappa_{\rho NN}$ | 1.99 |
| | | 3.38 | | 2.34 | | 3.53 | | 2.35 |
| | | 2.11 | | 2.65 | | 2.35 | | 2.26 |
| $a_0$ | $g_{a_0 NN}$ | 1.57 | – | – | $g_{a_0 NN}$ | 0.68 | – | – |
| | | 3.33 | – | – | | 2.55 | – | – |
| | | 0.93 | – | – | | 0.18 | – | – |
| $K^*$ | $g_{K^* N\Lambda}$ | -21.65 | $\kappa_{K^* N\Lambda}$ | -0.43 | $g_{K^* N\Lambda}$ | -21.58 | $\kappa_{K^* N\Lambda}$ | -0.43 |
| | | -21.99 | | -0.44 | | -23.23 | | -0.43 |
| | | -5.90 | | -0.44 | | -6.52 | | -0.43 |

TABLE V. Effective couplings $[g \cdot F(q^2)]$ to the nucleon on the mass shell and at threshold. In the first two columns we give the lower and upper values from Table IV. The SU(3) predictions use the given values for $g_{\pi NN}$, $g_{\rho NN}$, and $\kappa_{\rho NN}$ and include symmetry breaking on the level of 20% [40,5].

| | $q^2$ | KA84 | SM95 | Others | SU(3) |
|---|---|---|---|---|---|
| $g_{\pi NN}$ | $m^2$ | 13.05 | 13.05 | 13.14, [a] 13.41 [b] | 13.3 |
| | $q_s^2$ | 12.56–12.69 | 12.62–12.70 | – | – |
| $g_{\eta NN}$ | $m^2$ | 1.08–2.39 | 0.18–1.33 | 2.6–5.8, [c] 2.24, [d] | 2.75–5.0 |
| | $q_s^2$ | 0.57–1.26 | 0.10–0.77 | – | – |
| $g_{KN\Lambda}$ | $m^2$ | -(6.06–6.56) | -(6.10–6.36) | -14.78, [e] -10.96 [f] | -(10.3–16.7) |
| | $q_s^2$ | -(2.19–2.62) | -(2.17–2.84) | -5.35 [f] | – |
| $g_{\rho NN}$ | $m^2$ | 2.11–3.38 | 2.35–3.37 | 3.14, [b] 2.63 [g] | 2.66 |
| | $q_t^2$ | 2.07–2.11 | 1.98–2.35 | 2.67 [b] | – |
| $\kappa_{\rho NN}$ | $q_t^2$ | 2.14–2.65 | 1.99–2.35 | 2.25, [b] 3.71 [g] | 3.71 |
| $g_{a_0 NN}$ | $m^2$ | 0.75–3.33 | 0.18–2.55 | – | – |
| | $q_t^2$ | 0.53–0.75 | 0.18–0.30 | – | – |
| $g_{K^*N\Lambda}$ | $m^2$ | -(5.90–21.99) | -(6.52–23.23) | -(18.87–21.36), [e] -9.39 [f] | -(3.69–5.53) |
| | $q_t^2$ | -(4.44–7.94) | -(3.57–7.53) | – | – |
| $\kappa_{K^*N\Lambda}$ | $q_t^2$ | -0.44 | -0.43 | -(0.43–0.72), [e] 0.59 [f] | (1.48–2.23) |

[a]Reference [4].
[b]Reference [17].
[c]Reference [5].
[d]Reference [35].
[e]Reference [39].
[f]Reference [32].
[g]Reference [34].

eters for this state, it is not found anymore in the latest analysis of Arndt *et al.* [4]. The same is true for our fits, where the second $D_{13}$ resonance is found at 1.9 GeV. Since Batinić *et al.* [6] find two resonances in this energy range (at 1.817 and 2.048 GeV), the parameters given here have to be treated with the same caution as in the case of the $P_{13}(1720)$. Furthermore, we cannot reliably determine the parameters of the second $D_{13}$ resonance, since we only include data up to 1.9 GeV. Accordingly, we find no agreement between the different fits for the couplings and especially the $z$ parameters.

#### 2. Isospin-$\frac{3}{2}$ resonances

*a*. $S_{31}$. Our values are similar to those given by [4,33], whereas Manley and Saleski find the $S_{31}(1620)$ resonance at 1.672 GeV with a $\pi N$ partial width of 9%. The reason for this might be the $\pi\pi N$ approximation used in this work. Since Manley and Saleski find two strong channels for the $\pi\pi N$ decay ($\pi\Delta \approx 62\%$ and $\rho N \approx 25\%$), one cannot expect to obtain a good description of this decay by an effective $\zeta$ meson. This problem does not depend on the form factors used, as can be seen from the similar values in all fits.

*b*. $P_{31}$. As discussed in Sec. V B, we do not include a resonance in this channel. The data are only fitted up to 1.7 GeV; no resonance appears within this range [apart from a one-star candidate $P_{31}(1744)$ given by Manley and Saleski [3]].

This is an indication of how well the nonresonant background is described in our model. For all fits we find that we

TABLE VI. Values of the fitted cutoff parameters $\Lambda$. KA84 results are given in the first three rows (KA84-pp, KA84-ee, and KA84-pt); below are the results using SM95 (SM95-pp, SM95-ee, and SM95-pt).

| | Value [GeV] | | Value [GeV] | | Value [GeV] | | Value [GeV] |
|---|---|---|---|---|---|---|---|
| $\Lambda_N$ | 1.18 | $\Lambda_{1/2}$ | 1.59 | $\Lambda_{3/2}$ | 1.04 | $\Lambda_t$ | 0.90 |
| | 1.29 | | 1.82 | | 1.15 | | 0.92 |
| | 1.21 | | 1.72 | | 1.06 | | 0.71 |
| $\Lambda_N$ | 1.24 | $\Lambda_{1/2}$ | 1.36 | $\Lambda_{3/2}$ | 1.06 | $\Lambda_t$ | 0.88 |
| | 1.30 | | 1.71 | | 1.14 | | 0.88 |
| | 1.23 | | 1.24 | | 1.06 | | 0.70 |

TABLE VII. Resonance masses and couplings ($I=\frac{1}{2}$, $S=\frac{1}{2}$) as obtained in other models. For each resonance we list in lines one to five the values of Cutkosky *et al.* [1], Höhler *et al.* [2], Arndt *et al.* [4], Manley and Saleski [3], and Batinić *et al.* [6]. Furthermore, the $S_{11}$ parameters from [7] (line 6) and [33] ($K$-matrix result, line 7) are given. Only in [3] a $K\Lambda$ decay was included.

| | $M$ | $\Gamma_{\text{tot}}$ | $\Gamma_{\pi N}$ | | $\Gamma_{\zeta N}$ | | $\Gamma_{\eta N}$ | | $\Gamma_{K\Lambda}$ | |
|---|---|---|---|---|---|---|---|---|---|---|
| $L_{2I,2S}$ | [GeV] | [MeV] | [MeV] | % | [MeV] | % | [MeV] | % | [MeV] | % |
| $S_{11}(1535)$ | 1.550 | 240 | 120 | 50 | – | – | – | – | – | – |
| | 1.526 | 120 | 46 | 38 | – | – | – | – | – | – |
| | 1.535 | 66 | 20 | 31 | – | – | – | – | – | – |
| | 1.534 | 151 | 77 | 51 | 10 | 5 | 66 | 43 | 0 | 0 |
| | 1.553 | 182 | 84 | 46 | 7 | 4 | 91 | 50 | – | – |
| | 1.547 | 162 | 66 | 41 | 6 | 4 | 89 | 55 | – | – |
| | 1.534 | 125 | 53 | 42 | 19 | 15 | 54 | 43 | – | – |
| $S_{11}(1650)$ | 1.650 | 150 | 98 | 65 | – | – | – | – | – | – |
| | 1.670 | 180 | 110 | 61 | – | – | – | – | – | – |
| | 1.667 | 90 | 90 | 100 | – | – | – | – | – | – |
| | 1.659 | 173 | 154 | 89 | 13 | 8 | 6 | 3 | 0 | 0 |
| | 1.652 | 202 | 160 | 79 | 16 | 8 | 26 | 13 | – | – |
| | 1.695 | 293 | 226 | 77 | 67 | 23 | – | – | – | – |
| | 1.690 | 229 | 149 | 65 | 23 | 10 | 57 | 25 | – | – |
| $S_{11}(2090)$ | 2.180 | 350 | 63 | 18 | – | – | – | – | – | – |
| | 1.880 | 95 | 9 | 9 | – | – | – | – | – | – |
| | 1.712 | 184 | 70 | 38 | – | – | – | – | – | – |
| | 1.928 | 414 | 43 | 10 | 369 | 90 | 2 | 0 | 0 | 0 |
| | 1.812 | 405 | 130 | 32 | 186 | 46 | 89 | 22 | – | – |
| $P_{11}(1440)$ | 1.440 | 340 | 231 | 68 | – | – | – | – | – | – |
| | 1.410 | 135 | 69 | 51 | – | – | – | – | – | – |
| | 1.467 | 440 | 299 | 68 | – | – | – | – | – | – |
| | 1.462 | 391 | 270 | 69 | 121 | 31 | 0 | 0 | 0 | 0 |
| | 1.439 | 437 | 271 | 62 | 166 | 38 | 0 | 0 | – | – |
| $P_{11}(1710)$ | 1.700 | 90 | 18 | 20 | – | – | – | – | – | – |
| | 1.723 | 120 | 14 | 12 | – | – | – | – | – | – |
| | – | – | – | – | – | – | – | – | – | – |
| | 1.717 | 478 | 45 | 9 | 249 | 52 | 10 | 2 | 175 | 37 |
| | 1.729 | 180 | 40 | 22 | 130 | 72 | 11 | 6 | – | – |

overestimate the size of the real part of $P_{31}$ for energies around 1.35 GeV. Since the background is dominated by the Born terms and $\rho$ exchange in this region, an improvement of the description in this channel could only be achieved by reducing the quality of the fit in other channel(s).

Pearce and Jennings found that the same deviations only occur within the $K$-matrix approach, but not in other frameworks [17]. From this we conclude that for a better description of the data in this channel one would need to go beyond the $K$-matrix approximation.

*c*. $P_{33}$. As expected, all fits lead to the same parameters for the $P_{33}(1232)$. The numbers are slightly lower than in other works. In Sec. VI A this has already been shown to be the consequence of the $\rho NN$ form factor used in our calculation, which enforces a smaller $\rho NN$ coupling than usual. The fits try to compensate for this by lowering the mass and the width of the $P_{33}(1232)$.

The second resonance in this channel, the $P_{33}(1600)$, can be clearly seen in the $\pi N \to \pi\pi N$ channel, whereas its contribution to the $\pi N$-phase shift is negligible. Despite the discrepancy between the inelasticities from KA84/SM95 and the $\pi N \to \pi\pi N$ cross section, the couplings of the $P_{33}(1600)$ are well determined and comparable to the values given by Manley and Saleski ($m_R = 1.706$ GeV, $\Gamma_{\text{tot}} = 430$ MeV).

In contrast to the $I=\frac{1}{2}$ case, the $z$ parameters are very well determined for the $P_{33}(1232)$. As Fig. 5 shows, this is due to the strong offshell contribution to the $S_{31}$ partial wave. Since the off-shell part of the coupling is governed by the $z$ parameters, the high sensitivity of the fits is easily understood. Only a few extractions of $z_\pi$ for $P_{33}(1232)$ have been performed so far. Olsson and Osypowski [36] have used both $\pi N$-scattering and pion-photoproduction data. They found $z_\pi = -0.45$ ($\pi N$) and $z_\pi = -0.29$ (photoproduction). In another analysis of $\gamma N \to \pi N$ Davidson *et al.* [37] deduced $z_\pi = -0.24$. All these values are in good agreement with the results of our fits [$-(0.33$–$0.38)$ for KA84 and $-(0.31$–$0.35)$ for SM95], especially since the corresponding off-shell contributions are affected by rescattering.

*d*. $D_{33}$. Similar to the $S_{31}$ channel we find a resonance with a weak coupling to $\pi N$. Therefore, the parameters of the $D_{33}(1700)$ are determined by the $\pi N \to \pi\pi N$ data. Accordingly [as for the $S_{31}(1620)$], the masses we find are

TABLE VIII. Same as Table VII, but for the $I=\frac{1}{2}$, $S=\frac{3}{2}$ resonances.

| $L_{2I,2S}$ | $M$ [GeV] | $\Gamma_{\text{tot}}$ [MeV] | $\Gamma_{\pi N}$ [MeV] | % | $\Gamma_{\zeta N}$ [MeV] | % | $\Gamma_{\eta N}$ [MeV] | % | $\Gamma_{K\Lambda}$ [MeV] | % |
|---|---|---|---|---|---|---|---|---|---|---|
| $P_{13}(1720)$ | 1.700 | 125 | 13 | 10 | – | – | – | – | – | – |
| | 1.710 | 190 | 27 | 14 | – | – | – | – | – | – |
| | 1.820 | 354 | 57 | 16 | – | – | – | – | – | – |
| | 1.717 | 383 | 50 | 13 | 333 | 87 | 0 | 0 | 0 | 0 |
| | 1.720 | 244 | 44 | 18 | 200 | 82 | 1 | 0.4 | – | – |
| $D_{13}(1520)$ | 1.525 | 120 | 70 | 58 | – | – | – | – | – | – |
| | 1.519 | 114 | 62 | 54 | – | – | – | – | – | – |
| | 1.515 | 106 | 65 | 61 | – | – | – | – | – | – |
| | 1.524 | 124 | 73 | 59 | 51 | 41 | 0 | 0 | 0 | 0 |
| | 1.522 | 132 | 73 | 55 | 59 | 45 | 1 | 0.1 | – | – |
| $D_{13}(1700)$ | 1.675 | 90 | 10 | 11 | – | – | – | – | – | – |
| | 1.731 | 110 | 9 | 8 | – | – | – | – | – | – |
| | – | – | – | – | – | – | – | – | – | – |
| | 1.737 | 249 | 0 | 1 | 241 | 98 | 5 | 2 | 0 | 0 |
| | 1.817 | 134 | 12 | 9 | 103 | 77 | 19 | 14 | – | – |
| $D_{13}(2080)$ | 1.880 | 180 | 18 | 10 | – | – | – | – | – | – |
| | 2.081 | 265 | 16 | 6 | – | – | – | – | – | – |
| | – | – | – | – | – | – | – | – | – | – |
| | 1.804 | 447 | 104 | 23 | 224 | 50 | 119 | 27 | 0 | 0 |
| | 2.048 | 529 | 90 | 17 | 397 | 75 | 42 | 8 | – | – |

lower than those found by Manley and Saleski. As in the other cases, the partial widths are also smaller, but the branching ratios are in good agreement.

Again, the $z$ parameters are in good agreement between the different fits with the exceptions of KA84-pt and SM95-ee, where we find the same magnitude but opposite sign of $z_\pi$. This parameter is fixed mainly by the large contribution of the $D_{33}(1700)$ to the $P_{31}$ partial wave. Since we do not include a resonance in this channel, the value of $z_\pi$ depends on the interference with all background contributions and is therefore only well determined with respect to all these other couplings.

### C. Pole positions and residues

As we have already stated in the Introduction, we do not attempt to continue the $T$ matrix into the complex energy

TABLE IX. Same as Table VII, but for the $I=\frac{3}{2}$ resonances. Given are the values of Cutkosky *et al.* [1], Höhler *et al.* [2], Arndt *et al.* [4], and Manley and Saleski [3].

| $L_{2I,2S}$ | $M$ [GeV] | $\Gamma_{\text{tot}}$ [MeV] | $\Gamma_{\pi N}$ [MeV] | % | $\Gamma_{\zeta N}$ [MeV] | % | $\Gamma_{\eta N}$ [MeV] | % | $\Gamma_{K\Lambda}$ [MeV] | % |
|---|---|---|---|---|---|---|---|---|---|---|
| $S_{31}(1620)$ | 1.620 | 140 | 35 | 25 | – | – | – | – | – | – |
| | 1.610 | 139 | 49 | 35 | – | – | – | – | – | – |
| | 1.617 | 108 | 31 | 29 | – | – | – | – | – | – |
| | 1.672 | 154 | 14 | 9 | 140 | 81 | – | – | – | – |
| $P_{33}(1232)$ | 1.232 | 120 | 120 | 100 | – | – | – | – | – | – |
| | 1.233 | 116 | 116 | 100 | – | – | – | – | – | – |
| | 1.233 | 114 | 114 | 100 | – | – | – | – | – | – |
| | 1.231 | 118 | 118 | 100 | 0 | 0 | – | – | – | – |
| $P_{33}(1600)$ | 1.600 | 300 | 54 | 18 | – | – | – | – | – | – |
| | 1.522 | 220 | 46 | 21 | – | – | – | – | – | – |
| | – | – | – | – | – | – | – | – | – | – |
| | 1.706 | 430 | 53 | 12 | 377 | 87 | – | – | – | – |
| $D_{33}(1700)$ | 1.710 | 280 | 34 | 12 | – | – | – | – | – | – |
| | 1.680 | 230 | 46 | 20 | – | – | – | – | – | – |
| | 1.680 | 272 | 44 | 16 | – | – | – | – | – | – |
| | 1.762 | 599 | 81 | 14 | 518 | 86 | – | – | – | – |

TABLE X. Extracted resonance parameters using KA84. First line, KA84-pp; second, KA84-ee; third, KA84-pt. The signs of the couplings are given in brackets.

| $L_{2I,2S}$ | $M$ [GeV] | $\Gamma_{\text{tot}}$ [MeV] | $\Gamma_{\pi N}$ [MeV] | % | $\Gamma_{\zeta N}$ [MeV] | % | $\Gamma_{\eta N}$ [MeV] | % | $\Gamma_{K\Lambda}$ [MeV] | % |
|---|---|---|---|---|---|---|---|---|---|---|
| $S_{11}(1535)$ | 1.534 | 180 | 71(+) | 39 | 14(+) | 8 | 95(+) | 53 | – | – |
| | 1.542 | 175 | 67(+) | 38 | 7(+) | 4 | 101(+) | 58 | – | – |
| | 1.542 | 198 | 74(+) | 38 | 10(+) | 5 | 113(+) | 57 | – | – |
| $S_{11}(1650)$ | 1.694 | 212 | 157(+) | 74 | 38(+) | 18 | 1(−) | 0 | 16(+) | 8 |
| | 1.697 | 261 | 195(+) | 75 | 54(+) | 21 | 0(−) | 0 | 12(+) | 5 |
| | 1.701 | 278 | 205(+) | 74 | 61(+) | 22 | 1(−) | 0 | 11(+) | 4 |
| $P_{11}(1440)$ | 1.469 | 367 | 237(+) | 65 | 130(+) | 35 | 2.75 [a] | 0 | – | – |
| | 1.476 | 412 | 269(+) | 65 | 143(+) | 35 | 4.22 [a] | 0 | – | – |
| | 1.477 | 411 | 264(+) | 64 | 147(+) | 36 | 4.40 [a] | 0 | – | – |
| $P_{11}(1710)$ | 1.706 | 172 | 0(+) | 0 | 89(−) | 52 | 67(+) | 39 | 16(+) | 9 |
| | 1.696 | 123 | 0(+) | 0 | 71(−) | 58 | 19(+) | 15 | 33(+) | 27 |
| | 1.697 | 148 | 0(+) | 0 | 80(−) | 54 | 23(+) | 16 | 45(+) | 30 |
| $P_{13}(1720)$ | 1.790 | 384 | 84(+) | 22 | 259(+) | 67 | 36(+) | 9 | 5(+) | 1 |
| | 1.779 | 306 | 68(+) | 22 | 218(+) | 71 | 17(+) | 6 | 3(+) | 1 |
| | 1.803 | 480 | 107(+) | 22 | 324(+) | 68 | 44(+) | 9 | 5(+) | 1 |
| $D_{13}(1520)$ | 1.510 | 101 | 53(+) | 52 | 48(−) | 48 | 27 [b](+) | 0 | – | – |
| | 1.510 | 100 | 54(+) | 54 | 46(−) | 46 | 44 [b](+) | 0 | – | – |
| | 1.511 | 98 | 53(+) | 54 | 45(−) | 46 | 51 [b](+) | 0 | – | – |
| $D_{13}(1700)$ | 1.897 | 313 | 38(+) | 12 | 260(+) | 83 | 15(−) | 5 | 0(+) | 0 |
| | 1.888 | 303 | 41(+) | 14 | 259(+) | 85 | 3(−) | 1 | 0(+) | 0 |
| | 1.901 | 330 | 38(+) | 12 | 281(+) | 85 | 11(−) | 3 | 0(+) | 0 |
| $S_{31}(1620)$ | 1.601 | 150 | 48(+) | 32 | 102(−) | 68 | – | – | – | – |
| | 1.601 | 152 | 51(+) | 34 | 101(−) | 66 | – | – | – | – |
| | 1.582 | 162 | 33(+) | 20 | 129(−) | 80 | – | – | – | – |
| $P_{33}(1232)$ | 1.229 | 113 | 113(+) | 100 | – | – | – | – | – | – |
| | 1.229 | 113 | 113(+) | 100 | – | – | – | – | – | – |
| | 1.230 | 113 | 113(+) | 100 | – | – | – | – | – | – |
| $P_{33}(1600)$ | 1.675 | 406 | 52(+) | 13 | 354(+) | 87 | – | – | – | – |
| | 1.668 | 381 | 50(+) | 13 | 331(+) | 87 | – | – | – | – |
| | 1.674 | 384 | 50(+) | 13 | 334(+) | 87 | – | – | – | – |
| $D_{33}(1700)$ | 1.678 | 564 | 72(+) | 13 | 492(+) | 87 | – | – | – | – |
| | 1.678 | 512 | 68(+) | 13 | 444(+) | 87 | – | – | – | – |
| | 1.680 | 541 | 70(+) | 13 | 471(+) | 87 | – | – | – | – |

[a]The coupling $g_{\eta NR}$ is given instead of the partial width.
[b]Width in keV.

plane to locate the poles. The reason is mainly a technical difficulty in the effective Lagrangian approach. In this framework all Feynman diagrams would have to be calculated for complex energies and then decomposed into the partial waves. For the other models described in Sec. III the poles can be found more easily, since there the potential $V$ is determined in each partial wave independently and can, therefore, be chosen to be a function of $s$ only.

As a first approximation we estimate the location of the poles of the $T$ matrix following a method used by Höhler [16]. There the so-called *speed* of the amplitudes is used to determine the poles and residues directly from the PWA data. For details of the method see [16].

Starting point is the quantum mechanical consideration that the formation of an unstable excited state in a reaction leads to a time delay $Q$ between the outgoing wave packet and an undisturbed wave that can be calculated from the scattering amplitude [16,26]:

$$Q=-i\frac{dS}{dW}S^{-1}=2\left|\frac{dT}{dW}\right|, \quad W=\sqrt{s}. \tag{21}$$

The second equality holds for the case of elastic scattering. This can easily be generalized to the multichannel case. The speed is defined as

$$Sp(W)=\left|\frac{dT}{dW}\right|. \tag{22}$$

A peak of this speed corresponds in general to the formation

TABLE XI. Extracted resonance parameters using SM95. First line, SM95-pp; second, SM95-ee; third, SM95-pt. The signs of the couplings are given in brackets.

| $L_{2I,2S}$ | $M$ [GeV] | $\Gamma_{\text{tot}}$ [MeV] | $\Gamma_{\pi N}$ [MeV] | % | $\Gamma_{\zeta N}$ [MeV] | % | $\Gamma_{\eta N}$ [MeV] | % | $\Gamma_{K\Lambda}$ [MeV] | % |
|---|---|---|---|---|---|---|---|---|---|---|
| $S_{11}(1535)$ | 1.547 | 196 | 73(+) | 37 | 15(+) | 8 | 108(+) | 55 | – | – |
| | 1.544 | 156 | 63(+) | 40 | 9(+) | 6 | 84(+) | 54 | – | – |
| | 1.543 | 151 | 56(+) | 37 | 5(+) | 3 | 90(+) | 60 | – | – |
| $S_{11}(1650)$ | 1.689 | 234 | 173(+) | 74 | 48(+) | 21 | 1(−) | 1 | 13(+) | 6 |
| | 1.687 | 213 | 157(+) | 74 | 45(+) | 21 | 0(−) | 0 | 11(+) | 5 |
| | 1.692 | 209 | 155(+) | 74 | 41(+) | 20 | 0(−) | 0 | 13(+) | 6 |
| $P_{11}(1440)$ | 1.463 | 400 | 252(+) | 63 | 148(+) | 37 | 2.37 [a] | 0 | – | – |
| | 1.474 | 449 | 288(+) | 64 | 161(+) | 36 | 4.43 [a] | 0 | – | – |
| | 1.448 | 334 | 202(+) | 60 | 132(+) | 40 | 0.95 [a] | 0 | – | – |
| $P_{11}(1710)$ | 1.714 | 195 | 0(+) | 0 | 97(−) | 50 | 69(+) | 35 | 29(+) | 15 |
| | 1.700 | 142 | 0(+) | 0 | 83(−) | 58 | 40(+) | 28 | 19(+) | 13 |
| | 1.727 | 266 | 1(+) | 0 | 138(−) | 52 | 89(+) | 33 | 38(+) | 14 |
| $P_{13}(1720)$ | 1.772 | 340 | 76(+) | 22 | 223(+) | 66 | 37(+) | 11 | 4(+) | 1 |
| | 1.766 | 348 | 77(+) | 22 | 241(+) | 69 | 25(+) | 7 | 5(+) | 1 |
| | 1.771 | 344 | 74(+) | 22 | 241(+) | 70 | 24(+) | 7 | 5(+) | 1 |
| $D_{13}(1520)$ | 1.508 | 92 | 51(+) | 55 | 41(−) | 45 | 16 [b](+) | 0 | – | – |
| | 1.508 | 94 | 53(+) | 56 | 41(−) | 44 | 25 [b](+) | 0 | – | – |
| | 1.510 | 101 | 58(+) | 57 | 43(−) | 43 | 10 [b](+) | 0 | – | – |
| $D_{13}(1700)$ | 1.909 | 352 | 40(+) | 11 | 289(+) | 82 | 23(−) | 7 | 0(+) | 0 |
| | 1.882 | 217 | 25(+) | 12 | 171(+) | 79 | 21(−) | 10 | 0(+) | 0 |
| | 1.901 | 359 | 35(+) | 10 | 300(+) | 83 | 24(−) | 7 | 0(+) | 0 |
| $S_{31}(1620)$ | 1.595 | 148 | 42(+) | 28 | 106(−) | 72 | – | – | – | – |
| | 1.611 | 159 | 58(+) | 36 | 101(−) | 64 | – | – | – | – |
| | 1.598 | 150 | 44(+) | 29 | 106(−) | 71 | – | – | – | – |
| $P_{33}(1232)$ | 1.229 | 110 | 110(+) | 100 | – | – | – | – | – | – |
| | 1.230 | 110 | 110(+) | 100 | – | – | – | – | – | – |
| | 1.230 | 110 | 110(+) | 100 | – | – | – | – | – | – |
| $P_{33}(1600)$ | 1.690 | 431 | 60(+) | 14 | 371(+) | 86 | – | – | – | – |
| | 1.685 | 440 | 62(+) | 14 | 378(+) | 86 | – | – | – | – |
| | 1.686 | 405 | 59(+) | 15 | 346(+) | 85 | – | – | – | – |
| $D_{33}(1700)$ | 1.689 | 661 | 85(+) | 13 | 576(+) | 87 | – | – | – | – |
| | 1.686 | 669 | 88(+) | 13 | 581(+) | 87 | – | – | – | – |
| | 1.675 | 547 | 70(+) | 13 | 477(+) | 87 | – | – | – | – |

[a]The coupling $g_{\eta NR}$ is given instead of the partial width.
[b]Width in keV.

of a resonance state. For the $\pi N$ scattering this is always the case except for the cusp in the $S_{11}$ partial wave that is due to the opening of the $\eta N$ decay channel. Resonance parameters can therefore [with the exception of the $S_{11}(1535)$] also be obtained from *speed plots* that show $Sp(W)$ vs $W$.

Following [16] we now assume the $T$ matrix to be of the form

$$T(W)=T_{\text{back}}(W)+\frac{R\Gamma e^{i\Phi}}{m_R-W-i\Gamma/2} \tag{23}$$

in the vicinity of a resonance [=maximum of $\text{Sp}(W)$]. Here $m_R-i\Gamma/2$ is the location of the pole in the complex energy plane and $R\Gamma e^{i\Phi}$ is the residue. $T_{\text{back}}(W)$ is the background amplitude coming from nonresonant contributions. If the energy dependence of $T_{\text{back}}$ can be neglected, the speed depends only on the resonance parameters $m_R$, $\Gamma$, $R$, and $\Phi$. Using $T_{\text{back}}=\text{const}$ we find

$$\frac{dT}{dW}=\frac{R\Gamma e^{i\Phi}}{(m_R-W-i\Gamma/2)^2},$$

$$\text{Sp}(W)=\frac{R\Gamma}{(m_R-W)^2+\Gamma^2/4}. \tag{24}$$

Our procedure is now as follows: first, we determine $m_R$, $\Gamma$, and $R$ by fitting the speed given in Eq. (24) to the calculated

TABLE XII. Fitted $z$ parameters of the spin-$\frac{3}{2}$ resonances. Notation as in Table IV.

| | KA84 | | | | SM95 | | | |
|---|---|---|---|---|---|---|---|---|
| | $z_{\pi N}$ | $z_{\zeta N}$ | $z_{\eta N}$ | $z_{K\Lambda}$ | $z_{\pi N}$ | $z_{\zeta N}$ | $z_{\eta N}$ | $z_{K\Lambda}$ |
| $P_{13}(1720)$ | 1.440 | 0.216 | 0.348 | −0.683 | −1.771 | −0.126 | −1.375 | −0.248 |
| | 1.150 | 0.180 | 0.877 | −0.865 | −0.379 | 0.142 | −2.597 | −1.471 |
| | −1.013 | −0.177 | −1.207 | −0.981 | −2.200 | −0.210 | −1.993 | −0.421 |
| $D_{13}(1520)$ | −0.601 | 0.399 | −1.383 | – | 0.423 | −0.653 | 0.783 | – |
| | −0.558 | 0.070 | −1.005 | – | 0.366 | −0.559 | 0.724 | – |
| | −0.565 | 0.122 | −1.135 | – | 0.352 | −0.171 | 0.823 | – |
| $D_{13}(1700)$ | 0.776 | 0.862 | 0.037 | −0.749 | −0.830 | 0.408 | −0.079 | −1.050 |
| | 0.523 | 0.722 | −0.198 | −0.536 | −0.886 | −1.113 | −0.264 | −1.980 |
| | −0.396 | −0.887 | −0.689 | −3.695 | −1.281 | −0.990 | 0.195 | −2.240 |
| $P_{33}(1232)$ | −0.333 | – | – | – | −0.324 | – | – | – |
| | −0.355 | – | – | – | −0.354 | – | – | – |
| | −0.383 | – | – | – | −0.306 | – | – | – |
| $P_{33}(1600)$ | 1.532 | 0.107 | – | – | 1.564 | 0.100 | – | – |
| | −0.694 | −0.006 | – | – | 0.844 | −0.143 | – | – |
| | −0.112 | −0.765 | – | – | 1.587 | 0.094 | – | – |
| $D_{33}(1700)$ | 0.627 | −0.215 | – | – | 0.588 | −0.206 | – | – |
| | 0.628 | −0.197 | – | – | −0.725 | −0.083 | – | – |
| | −0.679 | 0.249 | – | – | 0.628 | −0.212 | – | – |

partial waves and, second, use this input to fix $\Phi$ from $dT/dW$. In this way we can extract resonance parameters directly from the unitarized $T$ matrix, consistent with the method usually used to determine resonance parameters from experimental data.

Since in an effective Lagrangian model all background contributions are well determined, one might try to discard all $u$- and $t$-channel contributions to reduce $T_{\text{back}}(W)$ in Eq. (23). This would allow a better extraction of the resonance parameters in cases where the background is not energy independent. Unfortunately, because of rescattering, this does not work in the $K$-matrix approach. Even if we had a constant background $K_{\text{back}}$ we could not disentangle its contributions to the $T$ matrix from the resonant part.

The results of these fits are given in Tables XIII and XIV, together with the values obtained in other models. The agreement for the pole positions between the different models is in general better than for the mass and width values listed in Tables VII–IX.

Furthermore, we note again that the decay widths extracted in our fits and given in the Tables X and XI are the values at the resonance positions and that the energy-dependent width also includes the respective form factors. In contrast to this the imaginary part of the pole position is (in our case) the width of a Lorentz function (24) fitted to the speeds and therefore corresponds to the FHWM of the resonance. From this it is easy to understand that the width deduced from the pole positions is in general smaller than the value of the energy-dependent width on the resonance mass, since our form factors decrease the resonance contributions for energies away from the resonance mass.

For the $S_{11}(1535)$ the pole position cannot be determined from the speed plot, since a peak due to the opening of the $\eta N$ channel dominates in this energy region. For the $P_{33}(1600)$ and $D_{33}(1700)$ no parameters could be extracted because they only appear as a shoulder in the speed plots. A fit to a speed plot derived from the $\pi\pi N\to\pi\pi N$ elastic amplitude could be used for these two resonances, since the $\pi\pi N$-decay is their major decay branch ($\approx$ 85%). Furthermore, the resulting Argand plots for $dT/dW$ show that the assumption of a constant background is not justified in the cases of $P_{11}(1710)$, $P_{13}(1720)$, $S_{31}(1620)$, and $D_{33}(1700)$. For these resonances an analytic continuation of the entire $T$ matrix would be needed to determine the pole positions more reliably.

The good agreement of the pole parameters obtained from our model with the results of the other models again shows the ability of the effective Lagrangian approach to describe the data.

### D. Interdependences of parameters

At the end of this discussion we focus on the interdependences of different parameters as determined from the covariance matrix $[C]$ of the fits. To this end we extracted the coefficients of correlation given by

$$r_{ij}=\frac{C_{ij}}{\sqrt{C_{ii}C_{jj}}}. \tag{25}$$

In contrast to the covariances $C_{ij}$, the $r_{ij}$ are restricted to values between $-1$ and 1 and therefore give a measure of the correlation that is independent of the individual variances $C_{ii}$ of the parameters. The most pronounced correlations are found for the following cases.

(i) As expected, the different parameters of a specific resonance (like mass and width) are strongly ($|r|\approx$ 0.6–0.9) correlated with themselves. The same is true for cases where

TABLE XIII. Values for the resonance poles and residues for the $I=\frac{1}{2}$ resonances compared to the results of other calculations. Shown are the range values of the three fits using KA84 (first line) and SM95 (second line) together with the values of Cutkosky *et al.* [1], Höhler [16], and Arndt *et al.* [4] in the following lines, respectively.

| | $M$ [GeV] | $\Gamma$ [MeV] | $R\Gamma$ [MeV] | $\Phi$ [deg] |
|---|---|---|---|---|
| $S_{11}(1535)$ | [a] | – | – | – |
| | [a] | – | – | – |
| | 1.510 | 260 | 120 | 15 |
| | 1.487 | – | – | – |
| | 1.501 | 124 | 31 | -12 |
| $S_{11}(1650)$ | 1.660–1.669 | 137–166 | 30–40 | -(38–48) |
| | 1.656–1.661 | 110–121 | 25–27 | -(53–59) |
| | 1.640 | 150 | 60 | -75 |
| | 1.670 | 163 | 39 | -37 |
| | 1.673, 1.689 [b] | 82, 192 | 22, 72 | 29, -85 |
| $P_{11}(1440)$ | 1.371–1.373 | 164–176 | 46–52 | -(84–87) |
| | 1.357–1.362 | 143–155 | 37–42 | -(94–95) |
| | 1.375 | 180 | 52 | -100 |
| | 1.385 | 164 | 40 | – |
| | 1.346 | 176 | 42 | -101 |
| $P_{11}(1710)$ | 1.674–1.690 | 82–150 | 5–11 | 80–94 |
| | 1.659–1.680 | 63–139 | 6–12 | 90–95 |
| | 1.690 | 80 | 8 | 175 |
| | 1.690 | 200 | 15 | – |
| | 1.770 | 378 | 37 | -167 |
| $P_{13}(1720)$ | 1.677–1.681 | 150–153 | 14–15 | -(115–120) |
| | 1.663–1.671 | 140–147 | 12–14 | -(116–120) |
| | 1.680 | 120 | 8 | -160 |
| | 1.686 | 187 | 15 | – |
| | 1.717 | 388 | 39 | -70 |
| $D_{13}(1520)$ | 1.497–1.498 | 93–94 | 25 | -(29–32) |
| | 1.496 | 86–94 | 24–28 | -(28–30) |
| | 1.510 | 114 | 35 | -12 |
| | 1.510 | 120 | 32 | -8 |
| | 1.515 | 110 | 34 | 7 |
| $D_{13}(1700)$ | [a] | – | – | – |
| | [a] | – | – | – |
| | 1.660 | 90 | 6 | 0 |
| | 1.700 | 120 | 5 | – |
| | – | – | – | – |

[a]Pole positions could not be deduced from the speed plots.
[b]Arndt *et al.* find two distinct cases.

there are two resonances in a partial wave. Here we find a strong interdependence between the parameters of both resonances (especially in the $S_{11}$ and $P_{11}$ channels, $|r|\approx 0.8$).

(ii) The correlations between the parameters of the $S_{I1}$ and $P_{I1}$ resonances and the $z$ parameters of $P_{I3}$ and $D_{I3}$ resonances are also easy to understand. This has already been pointed out in Sec. VI B 2 for the case of $z_\pi$ of the $P_{33}(1232)$ (cf. Fig. 5). The same effect can be seen in other channels as well, even though the values for the $z$ parameters vary between the different fits. Therefore, this effect can be seen best in the correlations and not in the parameters themselves. The correlations of the $S_{31}(1620)$ parameters to the off-shell contributions of the $P_{33}(1600)$ and the $D_{33}(1700)$ are noticable. In the case of $I=\frac{1}{2}$ resonances the $P_{11}(1440)$ parameters exhibit large dependences from the $z$ parameters of $P_{13}(1720)$.

(iii) We also find a strong correlation between the $P_{11}(1440)$ and the parameters of the $S_{31}(1620)$ ($|r|\approx 0.7$). This surprising result is due to the $u$-channel contributions of the latter to the $P_{11}$ channel. Because the $P_{11}(1440)$ is a rather broad resonance, its parameters are influenced by this background that is most important for energies $\approx 1.5$ GeV.

(iv) Since in our model the background is given by only a few contributions, it is not independently fixed in the differ-

TABLE XIV. Same as in Table XIII but for the $I=\frac{3}{2}$ resonances.

| | $M$ [GeV] | $\Gamma$ [MeV] | $R\Gamma$ [MeV] | $\Phi$ [deg] |
|---|---|---|---|---|
| $S_{31}(1620)$ | 1.598–1.603 | 101–108 | 15–16 | -(105–113) |
| | 1.588–1.595 | 91–123 | 11–16 | -(108–113) |
| | 1.600 | 120 | 15 | -110 |
| | 1.608 | 116 | 19 | -95 |
| | 1.585 | 104 | 14 | -121 |
| $P_{33}(1232)$ | 1.208 | 93–94 | 47 | -(49–50) |
| | 1.209–1.210 | 92–93 | 46 | -48 |
| | 1.210 | 100 | 53 | -47 |
| | 1.209 | 100 | 50 | -48 |
| | 1.211 | 100 | 38 | -22 |
| $P_{33}(1600)$ | [a] | – | – | – |
| | [a] | – | – | – |
| | 1.550 | 200 | 17 | -150 |
| | 1.550 | – | – | – |
| | 1.675 | 386 | 52 | 14 |
| $D_{33}(1700)$ | 1.590–1.593 | 144–146 | 10 | -(46–49) |
| | 1.582–1.591 | 150–163 | 11–12 | -(47–53) |
| | 1.675 | 220 | 13 | -20 |
| | 1.651 | 159 | 10 | – |
| | 1.655 | 242 | 16 | -12 |

[a]Pole positions could not be deduced from the speed plots.

ent partial waves. Accordingly, we find some degree of interdependence between the nonresonant parameters, mainly between $g_{\pi,\eta NN}$, $g_{KN\Lambda}$, and the various $z$ parameters of the spin-$\frac{3}{2}$ resonances.

(v) The parameters of the $D_{13}(1700)$ show a rather large correlation to the couplings of other resonances. This indicates that the couplings of the $D_{13}(1700)$ are not well determined by the $D_{13}$ partial-wave data; instead they are determined through off-shell contributions of this resonance to the other partial waves. Since we find the $D_{13}(1700)$ at the highest energies we consider in this work (around 1.9 GeV), its parameters cannot be extracted reliably.

These considerations represent a further indication that the resonance parameters [with the exception of the $D_{13}(1700)$] are determined reliably in the present model. The unexpected correlations of $P_{11}(1440)$ to $S_{31}(1620)$ point to some ''hidden'' form factor dependence that is not obvious from the extracted parameters alone.

## VII. COMPARISON WITH THE $T$-MATRIX APPROXIMATION

So far, the $T$-matrix approximation has been used in most models for $\gamma,\pi N\to\eta N,K\Lambda$ [5,20,32,35]. In this ansatz the $T$ matrix is calculated *directly* from the lowest-order Feynman diagrams. For the resonance contributions the imaginary part of the amplitude is introduced by hand through the inclusion of a width in the propagators:

$$T_{fi}^{\alpha}=\frac{-m_R\sqrt{\Gamma_f^{\alpha}(s)\Gamma_i^{\alpha}(s)}}{s-m_R^2+im_R\sum_{\alpha',d}\Gamma_d^{\alpha'}(s)}. \tag{26}$$

Here $\Sigma_{\alpha',d}\Gamma_d^{\alpha'}(s)$ denotes the total decay width of the resonance summed over all quantum numbers $\alpha'$ and decay channels $d$. At first glance this expression is very similar to the one obtained in the $K$-matrix approach for the case of a single resonance contribution [see Eq. (17)]:

$$T_{fi}^{\alpha}=\left(\frac{K}{1-iK}\right)_{fi}^{\alpha}=\frac{-m_R\sqrt{\Gamma_f^{\alpha}(s)\Gamma_i^{\alpha}(s)}}{s-m_R^2+im_R\sum_{d}\Gamma_d^{\alpha}(s)}. \tag{27}$$

Here $K$ is the full $n\times n$ matrix. The difference from Eq. (26) is that the sum in the denominator runs over the possible decay channels only. If $K^{\alpha}$ contains contributions from different resonances and diagrams, then it is no longer possible to write $T_{fi}^{\alpha}$ in the form (27). Additionally, in the $T$-matrix approximation the background contributions are purely real, whereas in the $K$-matrix formalism also the imaginary parts of these amplitudes are generated.

Calculating the $T$ matrix using Eq. (26) violates unitarity, because all rescattering contributions to a reaction $i\to f$ via some intermediate state $d\neq i,f$ are neglected. To have a measure for this violation in a specific channel $\alpha$, it is useful to look at the following quantity:

$$\Delta T^{\alpha}=[\mathrm{Im}\ (T)-T^2]^{\alpha}, \tag{28}$$

which vanishes if unitarity is fulfilled. Again $T$ denotes an $n\times n$ matrix. One expects $\Delta T^{\alpha}$ to be negligible for channels where a single resonance gives the dominant contribution (e.g., $D_{13}$ and $P_{33}$ in $\pi N$ scattering), since there the expressions (26) and (27) agree very well. This can be seen from the lower panel of Fig. 16. There the imaginary parts of the

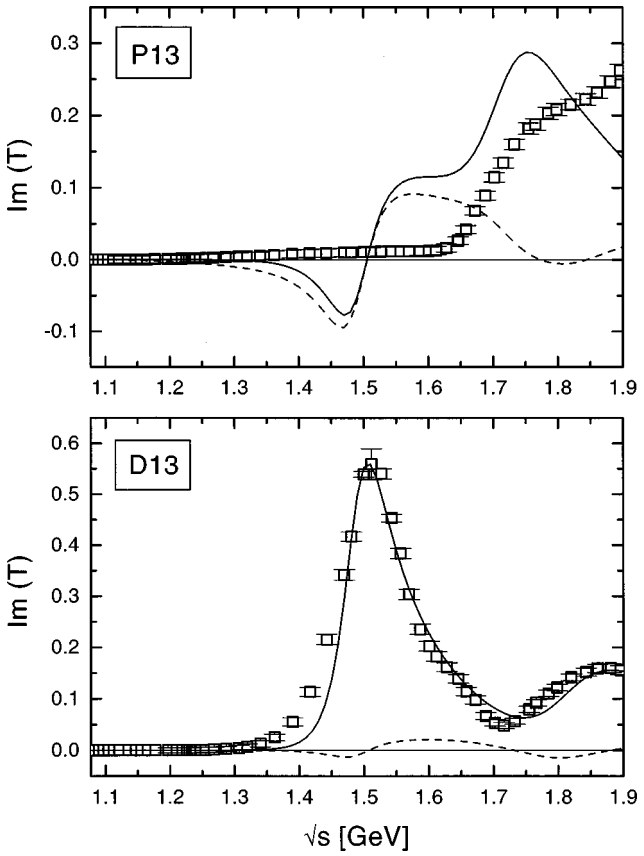


FIG. 16. Results using the $T$-matrix approximation (26). Shown are the imaginary parts of the $P_{13}$ and $D_{13}$ partial waves for $\pi N$ scattering (solid line) and the corresponding values $\Delta T^{\alpha}$ (dashed line) as described in Sec. VII. The data are taken from KA84.

$D_{13}$ partial wave and $\Delta D_{13}$ are shown for a calculation employing the $T$-matrix approximation. $\Delta D_{13}$ is small over the whole energy range and vanishes at the $D_{13}(1520)$ mass. We can further notice that the fit to the KA84 PWA is better than in the $K$-matrix formalism (cf. Fig. 1). This is due to the fact that in the case of the $T$ matrix, there are no contributions to the imaginary part from the background terms. Thus the real and imaginary parts of $T$ are ''decoupled'' and can be fitted independently.

The situation is completely different in the $P_{13}$ partial wave (Fig. 16, upper panel), where no satisfactory fit to the data can be found. Especially at energies around 1.5 GeV we find an additional structure when using the approximation (26) that is neither present in the data nor in the $K$-matrix results (Figs. 1 and 15). This structure is due to the contributions of the $D_{13}(1520)$ to the $P_{13}$ channel. As already discussed in Sec. IV B, the spin-$\frac{3}{2}$ resonances have off-shell contributions to various channels that can be adjusted using the $z$ parameters. In other words, the partial widths $\Gamma_d^{\alpha}(s)$ are in general not equal to zero for channels with quantum numbers that differ from those of the resonance $\alpha_R$. Only on the resonance position do we have

$$\Gamma_d^{\alpha\neq\alpha_R}(s=m_R^2)=0. \tag{29}$$

In the $T$-matrix approximation (26) the width in the propagator is taken to be $\Sigma_{\alpha',d}\Gamma_d^{\alpha'}(s)$ for all channels [Eq. (26)]

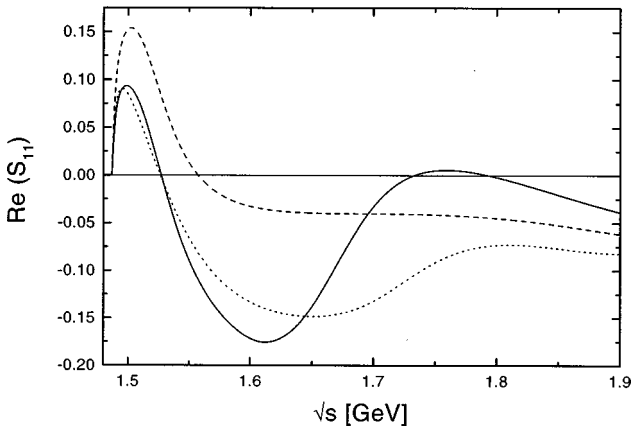


FIG. 17. Influence of the $S_{11}(1650)$ on the $\pi N\rightarrow\eta N$ amplitudes. Shown is the real part of $S_{11}$ for the $K$-matrix calculation using KA84-pt with (solid line) and without (dashed line) the $S_{11}(1650)$. For comparison we also show the $T$-matrix result (dotted line) using the same parameters.

and does not vanish on the resonance. Since the off-shell contributions of the spin-$\frac{3}{2}$ resonances to channels $\alpha\neq\alpha_R$ always change sign on the resonance position, the resulting amplitudes show structure as a function of $s$. For the $K$-matrix ansatz (27) this is not the case because in these channels both numerator and denominator go through zero on the resonance mass and the amplitude remains smooth. The artificial structures in the $T$-matrix approximations, introduced by spin-$\frac{3}{2}$ resonances, have already been observed in other effective Lagrangian calculations [15]. From this we conclude that a meaningful fit to *all* partial waves can only be done in the $K$-matrix approximation. In the fits using the $T$-matrix approach this shows up as an increased $\chi^2$ value, which is of the order of 15 for the use of the KA84 PWA (as compared to 2 in the $K$-matrix calculation).

As already mentioned, rescattering contributions with $d\neq i,f$ are neglected in the $T$-matrix approach. To illustrate the importance of these contributions, we show in Fig. 17 the real part of the $S_{11}$ partial wave for $\pi N\rightarrow\eta N$. The $K$-matrix calculations both with and without the $S_{11}(1650)$ resonance are compared to the $T$-matrix result. In the $K$-matrix approach the $S_{11}(1650)$ has a strong influence even though its $\eta N$ coupling is zero. In the $T$-matrix calculation this is not the case so that there all other couplings need to be adjusted to simulate the influence of the $S_{11}(1650)$. Especially the nonresonant parameters can therefore be viewed as *effective* couplings only.

## VIII. SUMMARY AND CONCLUSION

In this paper we have presented a unitary model for meson-nucleon scattering based on the $K$-matrix approximation. The potential is determined by contributions of the nucleon, $I=\frac{1}{2},\frac{3}{2}$ resonances, and meson exchanges in the $t$ channel. Effective Lagrangians are used to describe the couplings and form factors are taken into account at the vertices.

Within this approach we are able to describe all data of the reactions $\pi N\rightarrow\pi N$, $\pi N\rightarrow\pi\pi N$, $\pi^- p\rightarrow\eta n$, and $\pi^- p\rightarrow K^0\Lambda$ with the same set of parameters. The explicit inclusion of $\eta N$ and $K\Lambda$ final states enables us to extract the

decays of the resonances more reliably than by just using the $\pi N$ inelasticities. Our couplings and branching ratios are in good agreement with the values found in other calculations for the resonances coupling strongly to the $\pi N$ channel and show only minor deviations for the weakly coupling states. The pole positions and residues have been estimated and found to also be in good agreement with other results. Further work is clearly needed to analytically continue the $T$ matrix into the complex energy plane to locate the resonance poles more reliably. Nevertheless, we have shown that an effective Lagrangian ansatz is capable of describing the coupled channel dynamics adequately.

To estimate the systematic error in the determination of resonance parameters, we have performed six different analyses: (i) the $\pi N$ PWA KA84 and SM95 were used as an input, and (ii) the fits were done with three different combinations of form factors. We have found that we can reproduce the KA84 data somewhat better than the SM95 PWA, mainly because the latter is an energy-independent solution and exhibits larger scattering of the datapoints than the KA84 PWA.

One of the most important features of our analysis is that the nonresonant background is consistently generated from Feynman diagrams and thus the number of free parameters is reduced considerably. Furthermore, the background is not determined independently for each partial wave. In the fits this leads to a smaller $\rho NN$ coupling than usual. In order to circumvent this problem one would have to modify the $\rho$ contribution to obtain a Regge-like behavior. The smaller coupling of the $\rho$ in turn influences the masses and couplings of the resonances, especially for the $P_{33}(1232)$ and the $D_{13}(1520)$. Except for the $\rho NN$ coupling, we find that the other nucleon-meson couplings are reasonable and stable between the different fits.

A point of special interest is the $S_{11}(1535)$ due to its large $\eta N$-decay width. The extraction of accurate couplings would be very helpful. Unfortunately, we find a large systematic uncertainty coming from the uncertainty with respect to the form factors. Especially the mass of the resonance is not well constrained by the available $\pi^- p \to \eta n$ data. Since all fits and models describe the available data (see Fig. 11), only new measurements would help to clarify the situation. A search for a resonance pole of the $S_{11}(1535)$ within our approach would be very valuable in order to understand the nature of this resonance.

The $z$ parameters of the spin-$\frac{3}{2}$ resonances have been investigated systematically. For the $I=\frac{1}{2}$ case, these parameters exhibit large systematic errors and cannot be determined very accurately because the large number of resonances and open channels smear out the off-shell contributions. Accordingly, the fits are more stable for the $I=\frac{3}{2}$ resonances. The values for $z_\pi$ of the $\Delta$ that we find are in good agreement with those from previous analyses.

Our results indicate that a better fit to the $\pi N$ data could be possible with the use of form factors that are not symmetric around the resonance position. Especially for the spin-$\frac{3}{2}$ cases a significant improvement might be achieved with a functional form closer to the usual dipoles. This needs to be investigated in more detail.

The accuracy of the extracted parameters is limited mostly because of the poor quality of the $\eta N$ and $K\Lambda$ data. From these data the corresponding partial widths cannot be determined to better than $\approx$ 10–20 MeV. The resonance positions carry the same error. New measurements could improve the situation, but at the same time a better understanding of the differences between the $\pi N$ and the $\pi\pi N$ PWA is needed.

As already pointed out, another possible source of information is the photoproduction of mesons. Especially for the case of $\eta$ production high-quality data are available from recent measurements [38]. A combined analysis of the hadronic and electromagnetic reaction channels might put stricter limits on the resonance parameters.

## ACKNOWLEDGMENTS

One of the authors (U.M.) thanks the Institute for Nuclear Theory at the University of Washington for its hospitality and the U.S. Department of Energy for partial support during completion of this work. This work was supported by BMBF, GSI Darmstadt, and the U.S. DOE.

## APPENDIX A: EXTRACTION OF PARTIAL-WAVE AMPLITUDES

In this appendix we derive the relations between the Feynman matrix elements and the partial-wave decomposition of the meson-nucleon scattering. For the $\pi N$ case these relations are well known and given in standard textbooks [26,21]. We use the metric of Bjorken and Drell in the following [27]. $p$, $p'$, $q$, and $q'$ denote the four-momenta of the initial and final hadrons and the initial and final mesons. p, p′, q, and q′ are the corresponding absolute values of the three-momenta $\boldsymbol{p}$, $\boldsymbol{p}'$, $\boldsymbol{q}$, $\boldsymbol{q}'$.

### 1. Mesons of equal parity

If both initial and final mesons have the same parity, the Feynman amplitude for meson nucleon scattering is given by [$Q=(q+q')/2$ is the average of the meson momenta]

$$\mathcal{M}_{fi}=\bar{u}(p',s')(A+B\not{Q})u(p,s). \tag{A1}$$

In terms of Pauli spinors the scattering amplitude, on the other hand, can be written as [26]

$$\mathcal{F}=\tilde{A}+\tilde{B}\boldsymbol{\sigma}\cdot\hat{\boldsymbol{p}}'\boldsymbol{\sigma}\cdot\hat{\boldsymbol{p}},\quad \hat{\boldsymbol{p}}=\frac{\boldsymbol{p}}{\mathrm{p}},\quad \hat{\boldsymbol{p}}'=\frac{\boldsymbol{p}'}{\mathrm{p}'}, \tag{A2}$$

with the well-known decomposition

$$\mathcal{F}=\frac{1}{\sqrt{\mathrm{qq}'}}\sum_{l=0}^{\infty}[lT_{l-}+(l+1)T_{l+}]P_l + i\boldsymbol{\sigma}\cdot(\hat{\boldsymbol{p}}\times\hat{\boldsymbol{p}}')[T_{l+}-T_{l-}]P_l',$$

$$T_{l\pm}=\frac{\sqrt{\mathrm{qq}'}}{2}\int_{-1}^{1}d\cos\theta\,[\tilde{A}P_l(\cos\theta)+\tilde{B}P_{l\pm}(\cos\theta)]. \tag{A3}$$

The relation between the amplitudes $A$ and $B$ and their counterparts $\tilde{A}$ and $\tilde{B}$ can be derived by inserting the explicit

representation of the spinors and $\gamma$ matrices in Eq. (A1). Taking into account the different masses of the initial and final mesons leads to

$$\tilde{A}=\frac{\sqrt{(E'+m')(E+m)}}{8\pi\sqrt{s}}[A+B(\sqrt{s}-\bar{m})],$$

$$\tilde{B}=-\frac{\sqrt{(E'-m')(E-m)}}{8\pi\sqrt{s}}[A-B(\sqrt{s}+\bar{m})],$$

$$\bar{m}=\frac{m'+m}{2}. \tag{A4}$$

### 2. Mesons with different parity

For scattering of mesons with different parity the starting point is

$$\mathcal{M}_{fi}=\bar{u}(p',s')\gamma_5(A+B\not{Q})u(p,s),$$

$$\mathcal{F}=\tilde{A}\boldsymbol{\sigma}\cdot\hat{\boldsymbol{p}}'+\tilde{B}\boldsymbol{\sigma}\cdot\hat{\boldsymbol{p}}, \tag{A5}$$

with the same decomposition (A3) as in the equal-parity case. An analogous calculation yields the relations between $A,B$ and $\tilde{A},\tilde{B}$:

$$\tilde{A}=-\frac{\sqrt{(E'-m')(E+m)}}{8\pi\sqrt{s}}[A+B(\sqrt{s}+\partial m)],$$

$$\tilde{B}=\frac{\sqrt{(E'+m')(E-m)}}{8\pi\sqrt{s}}[A-B(\sqrt{s}-\partial m)],$$

$$\partial m=\frac{m'-m}{2}. \tag{A6}$$

### 3. Isospin decomposition

For the $I=1$ mesons $\pi$ and $\zeta$ we start from the standard projection operators [21]

$$P_{1/2}=\frac{1}{3}(1-\boldsymbol{t}\cdot\boldsymbol{\tau}),$$

$$P_{3/2}=\frac{1}{3}(2+\boldsymbol{t}\cdot\boldsymbol{\tau}), \tag{A7}$$

with the matrix elements $(a,b=\pi,\zeta)$

$$\langle b_j|P_{1/2}|a_i\rangle=\frac{1}{3}\tau_j\tau_i,$$

$$\langle b_j|P_{3/2}|a_i\rangle=\delta_{ji}-\frac{1}{3}\tau_j\tau_i, \tag{A8}$$

in a Cartesian basis. With the help of this all possible reactions can be written as

$$\langle b_j|T_{ba}|a_i\rangle=\frac{1}{3}\tau_j\tau_i T_{ba}^{1/2}+\left(\delta_{ji}-\frac{1}{3}\tau_j\tau_i\right)T_{ba}^{3/2} \tag{A9}$$

or explicitly as

$$\langle b^+p|a^+p\rangle=T_{ba}^{3/2},$$

$$\langle b^-p|a^-p\rangle=\frac{1}{3}(T_{ba}^{3/2}+2T_{ba}^{1/2}),$$

$$\langle b^-p|a^0n\rangle=\frac{\sqrt{2}}{3}(T_{ba}^{3/2}-T_{ba}^{1/2}),$$

$$\ldots,$$

with the factors being the corresponding Clebsch-Gordan coefficients.

For the pure $I=\frac{1}{2}$ reactions involving $\pi$ and $\zeta$ the projector is usually taken to be $P_{1/2}=\boldsymbol{\tau}$ [21]. This choice has the disadvantage that it does not agree with the Clebsch-Gordan coefficients for the different reactions channels. Therefore we choose instead $(a=\pi,\zeta,\ b=\eta,k)$

$$\langle b|P_{1/2}|a_i\rangle=\frac{-1}{\sqrt{3}}\tau_i,$$

$$\langle b|T_{ba}|a_i\rangle=\frac{-1}{\sqrt{3}}\tau_i T_{ba}^{1/2}. \tag{A10}$$

This has no influence on the calculated quantities, since in the end we convert our amplitudes to the normal convention.

## APPENDIX B: OBSERVABLES

For completeness we also list the formulas need for calculating the different observables from the partial waves. $P_l$ and $P_l'$ denote the Legendre polynomials and their derivatives.

Total cross sections $\sigma$:

$$\sigma=\frac{4\pi}{\mathrm{q}^2}\sum_{l=0}^{l_{\max}}[(l+1)|\tilde{T}_{l+}|^2+l|\tilde{T}_{l-}|^2]. \tag{B1}$$

Differential cross sections $d\sigma/d\Omega$ and final state polarizations $P$:

$$f=\frac{1}{\mathrm{q}}\sum_{l=0}^{l_{\max}}[(l+1)\tilde{T}_{l+}+l\tilde{T}_{l-}]P_l,$$

$$g=\frac{1}{\mathrm{q}}\sin\theta\sum_{l=0}^{l_{\max}}(\tilde{T}_{l+}-\tilde{T}_{l-})P_l',$$

$$\frac{d\sigma}{d\Omega}=|f|^2+|g|^2,\quad \frac{d\sigma}{d\Omega}P=-2\,\mathrm{Im}(f^*g). \tag{B2}$$

Here $\tilde{T}_{l\pm}$ denotes the partial-wave amplitude for a specific reaction. It is given as a sum over the contributing isospin channels:

$$\tilde{T}_{l\pm}=\sum_I p^I T_{l\pm}^I. \tag{B3}$$

The factors $p^I$ can be determined from Eqs. (A9) and (A10).

Inelastic cross section $\sigma_{\mathrm{inel}}$:

$$\sigma_{\rm inel}=\frac{4\pi}{\mathrm{q}^2}[\mathrm{Im}(T)-|T|^2]^{\alpha}_{\pi N}. \tag{B4}$$

## APPENDIX C: COUPLING CONSTANTS AND DECAY WIDTHS

In this appendix we list the formulas for the decay widths as calculated from the Lagrangians given in Sec. IV B. Here p denotes the three-momentum of the meson and nucleon, and $E_N$ and $E_\varphi$ the nucleon and meson energy, respectively:

$$\mathrm{p}=\frac{\sqrt{[s-(m_N+m_\varphi)^2][s-(m_N-m_\varphi)^2]}}{2\sqrt{s}},$$

$$E_N=\sqrt{\mathrm{p}^2+m_N^2},\quad E_\varphi=\sqrt{\mathrm{p}^2+m_\varphi^2}. \tag{C1}$$

For spin-$\frac{1}{2}$ resonances we have, for PS coupling,

$$\Gamma_{\pm}=\mathrm{ISO}\frac{g^2_{\varphi NR}}{4\pi}\mathrm{p}\frac{E_N\mp m_N}{\sqrt{s}}$$

and, for PV coupling,

$$\Gamma_{\pm}=\mathrm{ISO}\frac{g^2_{\varphi NR}}{4\pi(m_R\pm m_N)^2}\mathrm{p}\times\frac{2E_\varphi(E_NE_\varphi+p^2)-m_\varphi^2(E_N\pm m_N)}{\sqrt{s}}. \tag{C2}$$

The upper sign corresponds to decays of resonances into mesons with opposite parity [e.g., $P_{11}(1440)\rightarrow\pi N$]; the lower sign holds if both have the same parity [e.g., $S_{11}(1535)\rightarrow\pi N$]. ISO is the isospin factor; it is equal to 3 for decays into mesons with isospin one, and 1 otherwise.

Spin-$\frac{3}{2}$ resonances:

$$\Gamma_{\pm}=\frac{g^2_{\varphi NR}}{12\pi m_\pi^2}\mathrm{p}^3\frac{E_N\pm m_N}{\sqrt{s}}. \tag{C3}$$

Again, the upper sign is used if the resonance and meson are of opposite parity.


[1] R. E. Cutkosky, C. P. Forsyth, R. E. Hendrick, and R. L. Kelly, Phys. Rev. D **20**, 2804 (1979); **20**, 2839 (1979); R. E. Cutkosky, C. P. Forsyth, J. B. Babcock, R. L. Kelly, and R. E. Hendrick, in ''Baryon 1980,'' Proceedings of the 4th International Conference on Baryon Resonances, edited by N. Isgur (unpublished), p. 19.

[2] E. Pietarinen, Nucl. Phys. **B107**, 21 (1976); R. Koch, Nucl. Phys. **A448**, 707 (1986); Z. Phys. C **29**, 597 (1985); G. Höhler, F. Kaiser, R. Koch, and E. Pietarinen, ''Handbook of Pion-Nucleon Scattering,'' Physics Data 12-1, Karlsruhe, 1979 (unpublished).

[3] D. M. Manley, R. A. Arndt, Y. Goradia, and V. L. Teplitz, Phys. Rev. D **30**, 904 (1984); D. M. Manley and E. M. Saleski, *ibid.* **45**, 4002 (1992).

[4] SM95 and SP97 solutions of the VIRGINIA TECH PARTIAL-WAVE ANALYSIS, available via WWW from http://clsaid.phys.vt.edu/~CAPS. For further reference see, for example, R. A. Arndt, I. I. Strakovsky, R. L. Workman, and M. M. Pavan, Phys. Rev. C **52**, 2120 (1995); R. A. Arndt, R. L. Workman, Z. Li, and L. D. Roper, *ibid.* **42**, 1853 (1990).

[5] M. Benmerrouche, N. C. Mukhopadhyay, and J.-F. Zhang, Phys. Rev. D **51**, 3237 (1995).

[6] M. Batinić, I. Dadić, I. Šlaus, A. Švarc, B. M. K. Nefkens, and T.-S. H. Lee, Report No. 9703023, nucl-th/xxx.lanl.gov; M. Batinić, I. Dadić, I. Šlaus, A. Švarc, and B. M. K. Nefkens, Phys. Rev. C **51**, 2310 (1995).

[7] C. Sauermann, Ph.D. thesis, Darmstadt, 1996; C. Deutsch-Sauermann, B. Friman, and W. Noerenberg, Phys. Lett. B **409**, 51 (1997).

[8] Particle Data Group, Phys. Rev. D **54**, 1 (1996).

[9] S. Capstick and W. Roberts, Phys. Rev. D **49**, 4570 (1994).

[10] L. Ya. Glozman and D. O. Riska, Phys. Lett. B **366**, 305 (1996).

[11] R. Bijker, F. Iachello, and A. Leviatan, Phys. Rev. D **55**, 2862 (1997).

[12] N. Kaiser, T. Waas, and W. Weise, Nucl. Phys. **A612**, 297 (1997).

[13] M. Benmerrouche, R. M. Davidson, and N. C. Mukhopadhyay, Phys. Rev. C **39**, 2339 (1989).

[14] O. Scholten, A. Yu. Korchin, V. Pascalutsa, and D. Van Neck, Phys. Lett. B **384**, 13 (1996).

[15] T. Feuster and U. Mosel, Nucl. Phys. **A612**, 375 (1997).

[16] G. Höhler, $\pi N$ Newslett. **9**, 1 (1993).

[17] B. C. Pearce and B. K. Jennings, Nucl. Phys. **A528**, 655 (1991).

[18] L. M. Nath and B. K. Bhattacharyya, Z. Phys. C **5**, 9 (1980).

[19] P. van Nieuwenhuizen, Phys. Rep. **68**, 228 (1981).

[20] M. Sotona and J. Žofka, Prog. Theor. Phys. **81**, 160 (1989).

[21] T. Ericson and W. Weise, *Pions and Nuclei* (Calderon, Oxford, 1988).

[22] M. Gell-Mann and M. Levy, Nuovo Cimento **16**, 53 (1960).

[23] F. Klingl, N. Kaiser, and W. Weise, Nucl. Phys. **A624**, 527 (1997).

[24] R. D. Peccei, Phys. Rev. **181**, 1902 (1969).

[25] S. Nozawa, B. Blankleider, and T.-S.-H. Lee, Nucl. Phys. **A513**, 459 (1990); S. Nozawa and T.-S. H. Lee, *ibid.* **A513**, 511 (1990).

[26] M. L. Goldberger and K. M. Watson, *Collision Theory* (Wiley, New York, 1964).

[27] J. D. Bjorken and S.D. Drell, *Relativistic Quantummechanics* (Bibliographisches Institut, Mannheim, 1966).

[28] F. Hachenberg and H. J. Pirner, Ann. Phys. (N.Y.) **112**, 401 (1978).

[29] A. M. Green and S. Wycech, Phys. Rev. C **55**, 2167 (1997).

[30] R. M. Brown *et al.*, Nucl. Phys. **B153**, 89 (1979).

[31] D. H. Saxon *et al.*, Nucl. Phys. **B162**, 522 (1980).
[32] C. Bennhold, T. Mart, and D. Kusno, *Proceedings of the 4th CEBAF/INT Workshop on N* Physics* (World Scientific, Singapore, 1997).
[33] S. A. Dytman, T. P. Vrana, and T.-S. H. Lee, *Proceedings of the 4th CEBAF/INT Workshop on N* Physics* (World Scientific, Singapore, 1997).
[34] G. Höhler and E. Pietarinen, Nucl. Phys. **B95**, 210 (1975).
[35] L. Tiator, C. Bennhold, and S. S. Kamalov, Nucl. Phys. **A580**, 455 (1994).
[36] M. G. Olsson, Nucl. Phys. **B78**, 55 (1974); M. G. Olsson and E. T. Osypowski, *ibid.* **B87**, 399 (1975); Phys. Rev. D **17**, 174 (1978); Nucl. Phys. **B101**, 136 (1975).
[37] R. Davidson, N. C. Mukhopadhyay, and R. Wittman, Phys. Rev. D **43**, 71 (1991).
[38] B. Krusche *et al.*, Phys. Rev. Lett. **74**, 3736 (1995); **75**, 3023 (1995); Phys. Lett. B **358**, 40 (1995).
[39] R. A. Adelseck and B. Saghai, Phys. Rev. C **42**, 108 (1990).
[40] H. Thom, Phys. Rev. **151**, 1322 (1966).
[41] F. Bulos *et al.*, Phys. Rev. **187**, 1827 (1969).
[42] N. C. Debenham *et al.*, Phys. Rev. D **12**, 2545 (1975).
[43] W. Deinet *et al.*, Nucl. Phys. **B11**, 495 (1969).
[44] B. W. Richards *et al.*, Phys. Rev. D **1**, 10 (1970).
[45] J. Feltesse *et al.*, Nucl. Phys. **B93**, 242 (1975).
[46] R. D. Baker *et al.*, Nucl. Phys. **B141**, 29 (1978).
[47] T. M. Knasel *et al.*, Phys. Rev. D **11**, 1 (1975).